Chronic Empaglifozin treatment reduces myocardial infarct size in non-diabetic mice through STAT-3 mediated protection on microvascular endothelial cells and reduction of oxidative stress.

Chronic Empagliflozin Treatment Reduces Myocardial lnfarct Size in Nondiabetic Mice Through STAT-3-Mediated Protection on Microvascular Endothelial Cells and Reduction of Oxidative Stress

Panagiota Efstathia Nikolaou,[1] Panagiotis Efentakis,[1] Fairouz Abu Qourah,[1] Saveria Femminò,[2] Manousos Makridakis,[3] Zoi Kanaki,[4] Aimilia Varela,[5] Maria Tsoumani,[1] Constantinos H. Davos,[5] Constantinos A. Dimitriou,[5] Androniki Tasouli,[6] George Dimitriadis,[7] Nikolaos Kostomitsopoulos,[8] Coert J. Zuurbier,[9] Antonia Vlahou,[3] Apostolos Klinakis,[4] Maria F. Brizzi,[2] Efstathios K. lliodromitis,[10] and loanna Andreadou[1]

[1] Laboratory of Pharmacology, Faculty of Pharmacy, National and Kapodistrian University of Athens, Athens, Greece.
[2] Department of Medical Sciences, University of Turin, Turin, Italy.
[3] Biotechnology Laboratory, Centre of Basic Research, Biomedical Research Foundation of the Academy of Athens (BRFAA), Athens, Greece.
[4] Biomedical Research Foundation Academy of Athens, Athens, Greece.
[5] Cardiovascular Research Laboratory, Biomedical Research Foundation Academy of Athens, Athens, Greece.
[6] Onassis Cardiac Surgery Center, Athens, Greece.
[7] 2nd Department of Internal Medicine, Research Institute and Diabetes Center, National and Kapodistrian University of Athens, "Attikon" University Hospital, Athens, Greece.
[8] Academy of Athens Biomedical Research Foundation, Centre of Clinical Experimental Surgery and Translational Research, Athens, Greece.
[9] Amsterdam UMC, University of Amsterdam, Laboratory of Experimental Intensive Care and Anesthesiology, Department of Anesthesiology, Amsterdam Cardiovascular Sciences, Amsterdam Infection & Immunity, Amsterdam, The Netherlands.
[10] 2nd University Department of Cardiology, Medical School, National and Kapodistrian University of Athens, Athens, Greece.

Abstract

Aims: Empagliflozin (EMPA) demonstrates cardioprotective effects on diabetic myocardium but its infarct-sparing effects in normoglycemia remain unspecified. We investigated the acute and chronic effect of EMPA on infarct size after ischemia-reperfusion (I/R) injury and the mechanisms of cardioprotection in nondiabetic rnice. Results: Chronic oral administration of EMPA (6 weeks) reduced myocardial infarct size after 30 rnin/2 h I/R (26.5%±3.9% vs 45.8%±3.3% in the control group, $p<0.01$). Body weight, blood pressure, glucose levels, and cardiac function remained unchanged between groups. Acute administration of EMPA 24 or 4 h before I/R did not affect infarct size. Chronic EMPA treatrnent led to a significant reduction of oxidative stress biomarkers. STAT-3 (signal transducer and activator of transcription 3) was activated by Y(705) phosphorylation at the 10th minute of R, but it remained unchanged at 2 h of R and in the acute administration protocols. Proteornic analysis was employed to investigate signaling intermediates and revealed that chronic EMPA treatrnent regulates several pathways at re- perfusion, including oxidative stress and integrin-related proteins that were further evaluated. Superoxide dismutase and vascular endothelial growth factor were increased throughout reperfusion. EMPA pretreatrnent (24 h) increased the viability of human rnicrovascular endothelial cells in normoxia and on 3 h hypoxia/1 h reoxygenation and reduced reactive oxygen species production. In EMPA-treated murine hearts, CD31-NEGFR2-positive endothelial cells and the pSTAT-3(Y705) signal derived from endothelial cells were boosted at early reperfusion. Innovation: Chronic EMPA administration reduces infarct size in healthy mice via the STAT-3 pathway and increases the survival of endothelial cells. Conclusion: Chronic but not acute adrninistration of EMPA reduces infarct size through STAT-3 activation independently of diabetes mellitus.

Keywords: SGLT2 inhibitors, empagliflozin, infarct size, normoglycernia

lntroduction

Acute myocardial infarction (AMI) is one of the leading causes of death and disability worldwide. One- year mortality from AMI is on the decline; however, long- term mortality (1 year and beyond) remains significant (61). Therefore, cardioprotection on top of early reperfusion and the reduction of the incidence and severity of heart failure after AMI are existing clinical needs (17). So far, the translation of cardioprotective interventions from the bench to bedside has been disappointing (30). However, recently, a novel class of anti-diabetic drugs, the sodium-glucose cotransporter 2 (SGLT2) inhibitors have demonstrated remarkable benefits on the myocardium in a clinical setting.

The SGLT2 inhibitors are a new class of effective drugs against type 2 diabetes mellitus. These inhibitors not only improve management of hyperglycemia but, contextually, also reduce cardiovascular events, as demonstrated by the landmark clinical trials EMPA-REC, CANVAS, and Declare- TIMl (48, 66, 73) in which re-hospitalization for heart failure was reduced. Among the different clinically applicable SGLT2 inhibitors, empagliflozin (EMPA) is the most selective compound with more than 2500-fold SGLT2/SGLT1 selectivity (24). The EMPA treatment, as shown in the clinical trial EMPA-REG (73), decreased major cardiovascular events, including cardiovascular death and re-hospitalization for heart failure. These results reflect a reduction in the incidence of the acute coronary syndromes; however, our knowledge regarding the attenuation of myocardial necrosis on myocardial infarction is limited to preclinical studies.

Interestingly, several preclinical and clinical data support its direct cardioprotective and systemic effects, respectively (3). Direct improvement of cardiac calcium handling, through inhibition of myocardial Na^+/H^+ exchanger, and increase of myocardial levels of ketone bodies have been proposed as possible mechanisms to regulate calcium overload and energy consumption in heart failure (6, 62, 68). However, whether the reduction of myocardial infarct size is critical for the prophylactic role of EMPA against heart failure is still unknown. Well-described cardioprotective mechanisms in ischemia-reperfusion (I/R) injury, such as the signal transducer and activator of transcription 3 (STAT-3) (30), were shown to be favorably altered by EMPA (4) as we have reported that chronic administration of EMPA in a murine model of hyperglycemia reduced infarct size by activating the STAT-3 pathway (4).

In parallel, preclinical studies (16, 29, 55, 68) suggest the cardiovascular benefits of SGLT2 inhibitors in the absence of diabetes mellitus, and the DAPA-HF trial (42) was the first clinical trial indicating that SGLT2 inhibition can improve heart failure outcomes in nondiabetic patients. The scientific interest for the investigation of EMPAs actions independently of diabetes is increasing (31); however, the effect of EMPA on the healthy myocardium in vivo and the elucidation of the molecular mechanisms of cardioprotection are still pending. In terms of translational research, EMPA could be a valuable addition to the armamentarium for secondary prevention from AMI since this drug may attenuate myocardial cell death from I/R injury. Further, the direct impact of SGLT2 inhibition through EMPA on the myocardium remains debatable since the SGLT2 isoform is not expressed in the human and rodent myocardium (24, 63).

Based on all the data cited earlier, we sought to (i) investigate the effect of acute and chronic EMPA treatment on the nondiabetic myocardium in terms of rescuing I/R injury and (ii) explore the mechanisms implicated in cardioprotection.

Results

Acute administration of EMPA does not exert infarct size limitation properties

At first, we sought to investigate the acute effects of EMPA on the infarcted myocardium and determine whether one oral dose of EMPA given before the ischemic insult abrogates myocardial injury in healthy mice. We employed the first series of experiments in which 20 C57BL/6J male mice 12 weeks old (n = 5 per group) were equally randomized into 4 groups as follows: (i) Control 24 h: Oral administration of vehicle 24 h before 30 min of ischemia (I) and 2 h of reperfusion (30' I/2 h R); (ii) EMPA 24 h: Oral administration of EMPA 1O mg/kg 24 h before 30' I/ 2 h R; (iii) Control 4 h: Oral administration of vehicle 4 h before 30' I/2 h R; and (iv) EMPA 4 h: Oral administration of EMPA 1O mg/kg 4 h before 30' I/2 h. The schematic representation of the protocol is depicted in Figure 1A.

The dose of EMPA was selected based on our previous results in diabetic mice (4). The choice of the time points for EMPA administration was based on the observation that one single dose of EMPA increased myocardial energy capacity 4 h after its administration in diabetic animals (1). The 24 h correspond to more than six times the half-life of the drug in normal mice (f112 = 1.8 h) (15). This time point was implemented

to detect possible long-lasting effects of EMPA on a single dose of the drug. Acute administration of EMPA to healthy adult mice 24 or 4 h before sustained ischemia did not significantly affect the extent of infarct size compared with the respective control groups (Fig. 1B). The degree of the ischemic insult, as presented by the area at risk ratio (R/A), did not change among all four groups as shown in Figure 1C.

Chronic administration of EMPA in nondiabetic mice does not affect body weight, mean arterial pressure, glucose levels, and left ventricular function

Since EMPA did not reduce the infarct size acutely, we aimed at exploring the effects of chronic EMPA administration on nondiabetic animals in terms of infarct size reduction. Our second series of experiments included 16 C57BL/6J male mice 12 weeks old that were equally randomized to receive orally EMPA 10mg/kg/day (EMPA group) or vehicle (5% dimethyl sulfoxide [DMSO] in water for injection) for 6 weeks (control group). The schematic representation of the experimental protocol is depicted in Figure 2A. The regimen was chosen based on our previous study (4). Body weight was monitored weekly and revealed that EMPA does not alter body weight in nondiabetic mice (Fig. 2B). Fasting (8 h) blood glucose levels were determined at baseline, at day 21 of EMPA administration, and at the end of the treatment. The blood glucose measurements were performed 1 h after oral administration of EMPA since at this time point EMPA reaches the highest concentration in the blood (Tmax=1 h in normal mice) (59). Our results demonstrate that, in the absence of diabetes mellitus, EMPA did not significantly affect circulating blood glucose levels in comparison to the vehicle-treated group (Fig. 2C). Importantly, no evidence of hypoglycemia was observed. Mean arteria! blood pressure was measured at baseline and at the end of the EMPA treatment by using the tail-cuff system. Chronic ad- ministration of EMPA had no effect on diastolic, systolic, and mean arteria! blood pressure since equivalent values were re- corded between the two groups (p=NS) (Table 1). In parallel, echocardiography assessment at the aforementioned time points was performed and demonstrated no significant changes in left ventricular function and morphology between the control and EMPA groups, as shown by % fractional shortening(%FS) and the left ventricular radius to left ventricular posterior wall thickness ratio (r/h), respectively (Tables 2 and 3 and Supplementary Tables S1 and S2). We reported no signs of discomfort or distress with respect to the daily assessment of the animals.

Chronic administration of EMPA reduces infarct size and attenuates biomarkers of cardiac oxidative stress in absence of diabetes mellitus

To assess the infarct sparing properties of the 6-week EMPA treatment in the nondiabetic myocardium, the chronic cohort of EMPA administration (n=16) was subjected to 30' 1/2 h R. At the end of the reperfusion period, the hearts were excised, and triphenyl-tetrazolium chloride (TTC)-Evans Blue double staining was performed. Two mice were excluded from the analysis: one from the control group due to hemorrhage during the surgery and one from the EMPA group due to heart rupture during the staining by the cannula. Chronic EMPA administration significantly attenuated myocardial infarct size from 45.8%±3.3% to 26.5%±3.9% of the area at risk (n=7 per group, $p<0.01$) (Fig. 2D). In parallel, to determine the extent of the ischemic myocardium that was salvaged (13, 19), the salvage index was calculated. We noticed that EMPA treatment significantly increased the viable myocardium after 2 h of re- perfusion (n=7 per group, $p<0.01$) (Fig. 2D). Both groups had similar risk/all areas (p=NS) demonstrating comparable ischemic insult (Fig. 2E). Representative heart slices are shown in Supplementary Figure S1.

Then, we sought to identify whether oral administration of EMPA for 6 weeks attenuates cardiac oxidative stress by determining the biomarkers malondialdehyde (MDA) and protein carbonyls (PCs) in the myocardium as previously described (5, 21). Eighteen C57BL/6J male mice 12 weeks old were randomly divided into three groups (n=18, n=6 per group): (i) normoxia group, treated with vehicle; (ii) control group, treated with vehicle; (iii) and EMPA group, treated with 10 mg/kg/day with EMPA for 6 weeks per os. After 30' 1/1O' R or sham operation for the normoxia group, myocardial tissues were obtained and lysed, for MDA and PCs, respectively. The MDA and PCs levels were significantly increased on the ischemia/reperfusion stimuli ($p<0.05$ and $p<0.001$ vs. normoxia), and EMPA significantly attenuated both bio- markers of oxidative stress ($p<0.05$ and $p<0.001$, respectively, compared with control) (Fig. 2F, G). Our results clearly illustrate that chronic EMPA administration reduces the oxidative burden in the ischemic heart tissue at early reperfusion.

Chronic EMPA administration activates STAT-3 and has no effect on Akt and AMPKα signaling

We have previously reported that EMPA-mediated cardioprotective effects in mice with metabolic syndrome and increased glucose levels are associated with STAT-3 activation independently of the reperfusion injury

salvage kinase (RISK) pathway (4). Therefore, we investigated whether similar molecular mechanisms are involved in the mechanism of EMPAs cardioprotection in nondiabetic animals. In the third series of experiments, 16 mice were randomly divided to orally receive EMPA or vehicle for 6 weeks and were subjected to 30 min of ischemia. Myocardial biopsies from the ischemic left ventricle were obtained at the 10th minute and at 2 h of reperfusion for molecular analysis (n=4 per group) (Fig. 2A). Western blot analysis revealed a statistically significant increase in STAT-3(Y705) phosphorylation in the EMPA group at the 10th minute of reperfusion, compared with the control group at the same time point ($p<0.001$, Fig. 3B). STAT-3(Y705) phosphorylation did not differ between the two groups at 2 h of reperfusion (p=NS) (Fig. 3A, B and Supplementary Fig. S2A). In addition, STAT-3 expression did not change at the 10th minute and at 2 h of reperfusion in both groups (p=NS, Fig. 3A, B). Since the interaction between STAT-3 monomers may be modulated by the myocardial redox condition (69, 70), we further investigated STAT-3 dimerization. Additional mice were randomly divided into control and EMPA groups as mentioned earlier (n= 12, n=6 per group), and the ischemic part was obtained at the 10th minute of reperfusion. Since we observed the oxidative stress reduction by EMPA treatment at the 10th minute of reperfusion, this time point of reperfusion was chosen as the most suitable to investigate STAT-3 dimerization. The left ventricles of normoxic hearts were used as well (n=6). We employed a Western blot analysis under nonreducing conditions and we observed that chronic EMPA treatment significantly increases the phosphorylated monomer ($p<0.05$). Similarly, EMPA treatment led to a significant increase of the phosphorylated p(Y705)STAT-3/t STAT-3 dimer ($p<0.05$), deducing that EMPA enhances the dimerization state of STAT-3. Finally, we found that the expression of STAT-3 is not affected by the induction of I/R or the chronic EMPA treatment since the monomer and dimer tSTAT-3/ GAPDH ratios remained unchanged among the groups (Fig. 3C, D and Supplementary Fig. S2B).
Moreover, to investigate whether STAT-3 activation is de-pendent on RISK pathway activation in nondiabetic animals, we investigated the phosphorylation and expression of protein kinase B (Akt; S473) at the 10th minute and 2h of reperfusion. In line with our recently reported data in mice with metabolic syndrome (4), Akt expression and phosphorylation were similar between the EMPA and control groups (p=NS, Fig. 3E, F and Supplementary Fig. 2D). Previous reports regarding the cardiovascular effects of SGLT2 inhibitors, including canagliflozin and dapagliflozin, involve the activation of AMPKα kinase (29, 67, 72). However, herein we observed that chronic EMPA treatment did not increase AMPKα (Tl73) phosphorylation and expression (p=NS, Fig. 3E, F and Supplementary Fig. S2C).

Acute EMPA treatment does not activate STAT-3

Subsequently, to further elaborate our hypothesis that STAT-3 activation accounts for the cardioprotective effect of EMPA in myocardial I/R injury, we investigated whether acute administration of EMPA affects STAT-3 activation after I/R. In the next series of experiments, 24 mice (n=6 per group) were randomized to follow the acute administration protocol in which 1 dose of EMPA (10 mg/kg) was given 24 h or 4 h before 1/R (Fig. 1A). Myocardial tissue from the ischemic left ventricle was collected at the 10th minute of reperfusion, as this time point was affected by EMPA chronic treatment. One dose of EMPA before I/R injury did not alter STAT-3 phosphorylation when the drug was administered either 24 or 4 h before the ischemic insult (Fig. 4A, B and Supplementary Fig. S3). These results are consistent with our observation that acute EMPA administration does not reduce infarct size. Similar expression of STAT-3 between the EMPA groups and the respective control groups was detected (Fig. 4A, B and Supplementary Fig. S3).

Proteomic exploration of the biological processes of EMPA in vivo

Considering that STAT-3 activation was associated with the infarct-sparing effects of EMPA and was evident at the first minutes of reperfusion, we focused our further molecular investigation at the 10th minute of reperfusion. To explore possible biological processes that could explain the favorable effects of chronic EMPA treatment on myocardial infarct size reduction, we implemented a study of label- free proteomics in mouse heart tissue samples. To identify proteome alterations associated with EMPA treatment, liquid chromatography-tandem mass spectrometry (LC-MS/MS) analysis was performed on the protein lysate from myocardial biopsies of the ischemic area of the heart at the 10th minute of reperfusion (EMPA treatment for 6 weeks) (n=4 per group).
The LC-MS/MS analysis resulted in a total of 2364 proteins identified based on at least 2 peptides, and the average number of detected proteins were similar between the two groups (1396 for the control group and 1372 for the EMPA group). Lists of the assigned proteins by LC-MS/MS analysis are depicted in the Supplementary Table S4. After applying a threshold of 75%, 1368 proteins formed our dataset

(Supplementary Table S4) in which the Mann-Whitney test was applied between the two groups. Only the proteins that fulfilled the following criteria (i) statistically significant different (p:::; 0.05, Mann-Whitney test) or (ii) had a fold change of at least 2 (|fold change| :2: 2) were used for further analysis and visualization (Fig. 5B and Supplementary Fig. S4 and Supplementary Tables S3 and S4).
To assess the quality of the proteomics data in an unsupervised fashion, principal component analysis (PCA) was per- formed by employing different scaling techniques. Pareto scaling methodology offered an enhanced clustering capacity between the EMPA-treated and vehicle-treated group (Fig. 5A). We performed over-representation analysis, with the default parameters of the online gene set analysis tool WebGestalt (64, 65) (Pathway enrichment analysis and Wiki pathways as data base) for the set of our statistical significant or differentially expressed proteins.
We observed that of the statistically significant pathways (Benjamini-Hochberg corrected p-value ≤ 0.05, two-sided hypergeometric test) that were predicted to be deregulated, the majority were relevant to the mitochondrial respiratory chain (electron transport chain, oxidative phosphorylation), and regulation of oxidative stress (glutathione metabolism, oxidative stress), whereas cell adhesion (Alpha6-Beta4 Integrin Signaling Pathway; Rhoa, Grb2) was also among the top 10 molecular processes that were predicted to be represented by the changing proteins. STAT-3 has been associated in the literature with the regulation of oxidative stress, cell survival and migration, and angiogenesis (2). For this reason, from the pool of significant pathways revealed by the pathway enrichment analysis (Fig. 5C), we further investigated how the oxidative stress and the integrin signaling pathway could be related to the EMPAs cardioprotective mechanism.

Chronic treatment with EMPA upregulates vascular endothelial growth factor and superoxide dismutase 2 levels in murine nondiabetic hearts

To further investigate these signaling pathways, we employed an additional cohort of chronic EMPA administration (n=12 mice in total, n=6 per group) and the ischemic part of the myocardium was collected for RNA isolation on 30 min I/10 min reperfusion. Real-time polymerase chain reaction (RT-PCR) was performed and the mRNA levels of super- oxide dismutase 2 (Sod2), inducible nitric oxide synthase (Nos2), and NAPDH oxidase 2 (Nox2) as regulators of oxidative stress were determined. Moreover, proteomic analysis revealed that EMPA differentially regulates integrin-related proteins associated with Ras/GTPase/cytoskeleton axis (e.g., Rhoa, Rhoc, Rab5a, Cfl1) and growth factors signaling adaptors (Grb2) that are highly associated with vascular endothelial growth factor receptor 2 (VEGFR2) signaling (2). Therefore, we determined the mRNA expression of vascular endothelial growth factor α (Vegfα), β (Vegfβ) and vascular endothelial growth factor receptor 2 (Vegfr2). Endothelial nitric oxide synthase (Nos3) mRNA was measured as a functional endothelial marker.
Among the studied genes, Vegfβ and Sod2 mRNA were significantly upregulated in the EMPA group at the 10th minute of reperfusion (*p<0.05 vs. control; Fig. 5D and Supplementary Fig. S5), whereas the expression of all other genes remained unchanged (p=NS; Fig. 5D). The expression of SOD2 protein was evident at the 10th minute of reperfusion (n=6 per group) and 2 h of reperfusion (n=4 per group; p<0.05), whereas VEGF was increased at protein level at 2 h of reperfusion (n=4 per group) (*p<0.05 vs. control; Fig. 5E, F). The latter data support the hypothesis that chronic EMPA treatment induces endogenous detoxifying mechanisms and potentiates the survival and/or proliferation of endothelial cells at reperfusion in the nondiabetic myocardium.

EMPA treatment protects human microvascular endothelial cells against hypoxia/reoxygenation injury

Taking into account that VEGF is an endothelial- associated molecule, we focused our attention on the effect of EMPA on microvascular endothelial cells under normoxic and hypoxic conditions. Human microvascular endothelial cells (HMECs) were subjected to normoxia or hypoxia/ reoxygenation (H/R) stress and were treated with EMPA, 500 nM (4), or vehicle for 24 h before 3 h H/1 h R. In addition, and since STAT-3 underwent activation during early reperfusion, Stattic, a STAT-3 inhibitor, was used at 500 nM (7), to elucidate whether the EMPA mechanism of action is STAT-3 dependent. The 3-(4,5-Dimethylthiazol-2-yl)-2,5-diphenyl-tetrazolium bromide (MTT) assay on HMECs treated with EMPA under normoxic conditions showed increased viability of the cells compared with vehicle (n=8 replicates, p<0.05).
Moreover, under H/R conditions, EMPA treatment significantly increased cell viability in comparison to the vehicle-treated group (n=8 replicates, ****p<0.0001). The EMPA's protective effect was blunted by Stattic and EMPA co-treatment (****p<0.0001, EMPA group in comparison to EMPA co-treatment) (Fig. 6A). Stattic alone decreased cell viability in comparison to the H/R group (*p<0.05), and Stattic/EMPA co-

treatment had similar viability to H/R (p=NS) (Fig. 6A). Taken together, these results indicate that EMPA directly favors endothelial cell survival though a STAT-3 mediated mechanism.

EMPA treatment inhibits H/R-mediated ROS production in absence of STAT-3 activation

Subsequently, being aware of the protective effect of EMPA through oxidative stress reduction, we subjected HMECs to the same H/R protocol and we evaluated ROS production. EMPA and Stattic were used as in the in vitro H/R experiment described earlier. Long-term (24 h) treatment with EMPA led to a significant reduction of ROS- producing cells (**p<0.01), whereas Stattic treatment did not abrogate the EMPA effect (p=NS in comparison to EMPA) (Fig. 6B). Therefore, EMPA treatment can reduce oxidative stress in the absence of STAT-3 activation.

EMPA increases endothelial celI survival in vivo

On the basis of the pro-surviving effect of EMPA on microvascular endothelial cells in both normoxic and H/R conditions, we sought to verify whether this effect was also evident in vivo on chronic EMPA treatment. Therefore, 12 additional mice were randomized to receive EMPA or vehicle (n=3 per group) for 6 weeks. At the end of the treatment, mice were either sham operated or subjected to 30 min I and 10 min R. Fluorescence immunohistochemistry was per- formed on cardiac tissues derived from ischemic left ventricle and from sham-operated animals by using CD31 and VEGFR2 as endothelial cell markers (46). In addition, pSTAT-3(Y705) staining was used to explore the localization of the transcriptional factor activation. Representative immunofluorescence images and the integrated fluorescence density of the CD31/DAPI and VEGFR2/DAPI staining demonstrate that chronic EMPA administration increases CD31- and VEGFR2-positive cells in both the sham-operated group and at early reperfusion in comparison to their respective controls, indicating that the increased capillary density is independent of the I/R stress (Fig. 6C-E). Importantly, pSTAT-3(Y705) co-localized with CD31 and VEGFR2 in the I/R-affected myocardium, suggesting that this cardioprotective signal also derives from cardiac endothelial cells (Fig. 6C). The IDF of p(Y705)STAT-3/CD31 is significantly increased in the EMPA group compared with the control, which suggests that EMPA improves the survival of endothelial cells by activating STAT-3 (p<0.01; Fig. 6F).

Discussion

This study investigated the cardioprotective effect of acute and chronic EMPA administration in terms of infarct size reduction in nondiabetic mice. We employed an in vivo experimental model of myocardial infarction and we explored possible implicated mechanisms for the observed effects. Herein, we demonstrate that chronic but not acute administration of EMPA attenuates I/R injury through reduction of oxidative stress and STAT-3 activation and dimerization at the early reperfusion. Moreover, the cardioprotective effect of EMPA can be also attributed to the upregulation of de- toxification mechanisms and the VEGF pro-survival stimulus. The STAT-3-dependent improvement of microvascular endothelial cell survival also contributes to the alleviation of the reperfusion injury.

This study is the first to demonstrate that acute oral ad- ministration of EMPA 24 or 4 h in vivo before the ischemic insult does not result in significant reduction of myocardial infarct size. Similar effects were observed by Jespersen et al. (31a) and Uthman et al. (62) in an ex vivo rat/mouse model of myocardial I/R when EMPA was given 10--20 min before the induction of ischemia. Moreover, short-term perfusion of the nondiabetic heart with canagliflozin did not result in myocardial infarct size reduction (38). However, when canagliflozin was given at the fifth minute after the induction of ischemia in an in vivo nondiabetic rat model of myocardial infarction, the infarct size was significantly reduced (55). Distinct mechanisms of cardioprotection could be speculated among the SGLT2 inhibitors, and, therefore, future comparative studies are required to enlighten drug-specific effects and the exact timeframe of acute protection.

We first show in this study that a period of 6 weeks of treatment with EMPA in healthy mice significantly reduces infarct size and increases the extent of viable myocardium compared with the control group independently of glucose levels. These results corroborate with the important study by Lim et al. (38) in which chronic administration of canagliflozin for 4 weeks in nondiabetic rats significantly reduced myocardial infarct size ex vivo (38).

It is well established that SGLT2 inhibitors reduce blood glucose levels, blood pressure, and body weight in humans with type 2 diabetes mellitus (23, 47, 52, 66, 73) and in animal models mimicking such pathophysiology (4, 25, 51, 60). These effects have been partially attributed to glycosuria, and further

underlying mechanisms are under investigation (36). Notably, the biometric parameters (body weight, glucose levels, and arterial pressure) remained unaffected in healthy, nondiabetic animals in our study. Our results on glucose levels are consistent with previous studies regarding chronic administration of SGLT2 inhibitors in nondiabetic animals, showing no evidence of altered blood glucose levels (38, 68). As far as the body weight is concerned, our results are in line with a study in which dapagliflozin was given for 4 weeks after myocardial infarction in nondiabetic rats and no significant changes were observed (37). However, body weight was reduced on chronic administration of EMPA and canagliflozin in nondiabetic rats (38, 68), indicating that the choice of different anima! models and the dose of SGLT2 inhibitors could lead to variation between the observed effects. Moreover, herein we demonstrate that chronic administration of EMPA does not affect left ventricular function and contractility of the nondiabetic myocardium. In line with our data, chronic administration of EMPA did not alter cardiac function parameters in normoglycemic rats (68), indicating the safety of the drug for the nondiabetic myocardium on long-term treatment. Improvement in cardiac function is only apparent in the presence of co-morbidities, leading to hemodynamic and metabolic disorders as previously demonstrated by our (4) and other groups (16, 27, 51).

A burst of reactive oxygen species occurs at early reperfusion (53) and is a key regulator of cell death and myocardial infarct size (18). In our study, we measured MDA and PCs as established redox biomarkers (22) and also because these markers of lipid and protein oxidation have been previously recruited successfully to define the oxidative status of the myocardium (4, 19). We observed that chronic EMPA treatment significantly decreased the biomarkers mentioned earlier in myocardial tissues on I/R stress. This result is in agreement with previously reported data showing that EMPA directly inhibits the sodium-hydrogen exchanger (NHE) (6), and NHE depletion is related to oxidative stress reduction (54). Myocardial antioxidant effects have been also demonstrated for other SGLT2 inhibitors independently of diabetes (55).

As far as the cardioprotective mechanisms are concerned, we investigated the phosphorylation of STAT-3 on Y705, which been associated with cardioprotection during the first minutes of reperfusion (4). Increased p(Y705)STAT-3 was evident at the 10th minute of reperfusion, indicating its increased activity without significant alterations of its expression throughout reperfusion. STAT-3 is one of the main signaling molecules in the SAFE pathway and is considered a major mediator of cardioprotection, leading to a decrease in infarct size (11, 12, 30). Oxidative stress can modify the ability of STAT-3 to undergo phosphorylation and to act as a transcriptional regulator via dimerization (69, 70). Our results demonstrate that EMPA improves the formation of Y(705)STAT-3 dimers and, therefore, as the result of dimer formation, several anti-oxidant and antiapoptotic genes can be regulated via the STAT-3 canonical pathway (70, 74).

Notably, acute administration of EMPA does not affect the expression and activation of STAT-3 in our study. This is in line with the fact that infarct size was not reduced. The evaluation of STAT-3 activation in the acute EMPA proto- cols was performed in 12 week-old mice that were 6 weeks younger than the chronic cohorts. Therefore, we can safely exclude the possibility that the cardioprotective signaling is lost due to aging (10) and conclude that STAT-3 activation by EMPA is only related to infarct size reduction. Current results are in agreement with our previous study in hyperglycemic mice (4). Moreover, they further suggest that STAT-3 mediating cardioprotection is independent of the presence of diabetes mellitus. In line with our data, chronic administration of dapagliflozin in an experimental model of nondiabetic rats enhanced phenotypic switch of macrophages toward the M2 phenotype, reduced myofibroblast infiltration and consequently cardiac fibrosis after myocardial infarction through STAT-3 activation (37).

Although STAT-3 is activated on cardioprotective maneuvers as part of the SAFE pathway, a cross-talk between RISK and SAFE has been also postulated (28). However, in our study, EMPA did not alter the expression and the phosphorylation of Akt and AMPKα kinases neither at the 10th minute nor at 2 h of reperfusion, suggesting that the reduction of infarct size is due to activation of the SAFE signaling pathway independent of the RISK pathway and the AMPKα downstream effectors. This result is consistent with previous reports in which EMPA did not activate AMPK in human umbilical vein endothelial cells and in human aortic endothelial cells (41). Our results are dissimilar to the study of Sayour et al. (55), in which acute canagliflozin treatment induced Akt activation in infarcted hearts and the discrepancy may be attributed to the timeframe of the treatment.

To identify the biological pathways that are regulated at early reperfusion on chronic EMPA treatment, we performed proteomic analysis and to the best of our knowledge, this is the first time that such an analysis is performed for the investigation of the cardioprotective effect of SGLT2 inhibitors. We must mention herein that we could not determine STAT-3 in the proteomic dataset since it is well established that low abundant proteins are not easily identified with high- throughput and untargeted proteomic approaches (39). However,

global proteomic profiling enables the visualization of grossly affected cellular processes and provides hints for further and unbiased research. From the pathway enrichment analysis in this study, we sought to characterize those that could be related to STAT-3 signaling such as the regulation of oxidative stress and the pathway related to integrins.
Ten proteins of our curated dataset of statistically significant or differentially expressed proteins (Grb2, Cfl1, Rhoa, Fgg, Fgb, Gpcl, Rhoc, Mapk14, Rab5a, Hras) belong to the VEGF/VEGFR2 signaling network (2), which can potentiate and sustain angiogenesis or promote survival signaling for endothelial cells (8, 9). Our RT-PCR data showed the upregulation of Vegfβ in the EMPA-treated heart post-I/R, which was confirmed at protein level at 2 h of reperfusion. Increased VEGF by inflammation has been described to reduce infarct size through a preconditioning effect (43), and therefore the upregulation of VEGF by EMPA could represent a potential novel cardioprotective mechanism. The VEGF-related path- way has been also related to the protective action of another SGLT2 inhibitor, luseogliflozin, against renal fibrosis and capillary injury (71). Therefore, further studies could elucidate whether this molecular signal is a class effect ofSGLT2 inhibitors.
The oxidative stress regulation was evident from proteomics. Therefore, we confirmed that Sod2 mRNA levels and SOD2 protein were significantly increased in the EMPA- treated myocardium compared with the controls, indicating that EMPA increases the endogenous cardiac antioxidant capacity and renders the myocardium less susceptible to ROS-induced cell death (17, 22). Both VEGF and SOD2 are downstream effectors ofSTAT-3 (70, 74) and are associated with the cardioprotective effect of EMPA.
Based on our findings on integrin-related proteins over- representation, we subsequently shifted our focus on the effect of EMPA on microvascular endothelial cells. The EMPA increased HMEC's viability in normoxia and hypoxia, whereas we found that under hypoxic conditions the protective effects were STAT-3 dependent. We confirmed these findings in vivo by immunofluorescence staining of the EMPA-treated myocardium, as EMPA increases endothelial cells in the myocardium independently of I/R, whereas STAT-3 is found to be favorably activated in endothelial cells at the 10th minute of reperfusion. The STAT-3 and VEGF pathways have been already reported to have a mutual activatory relationship, because the VEGFR2 receptor is a tyrosine kinase receptor that can mediate STAT-3 activation in endothelial cells, whereas STAT-3 stands as a transcription factor of VEGF (9, 14). However, the mechanism by which EMPA increases endothelial cell proliferation in vivo before the ischemic insult is still under investigation and might rely on the other cellular populations in the myocardium such as smooth muscle cells and fibroblasts.
In conclusion, herein we provide evidence that chronic EMPA administration reduces cardiac oxidative stress and activates STAT-3 through its Y(705) phosphorylation and dimerization. In parallel, EMPA induces VEGF expression and improves endothelial cell survival in a STAT-3 dependent manner (Fig. 7). The increased proliferation of endothelial cells on EMPA treatment that was found as independent of 1/R requires further characterization and will be the topic of our future studies.

Limitations
In this study, we investigated the infarct-limiting effect of acute and chronic EMPA treatment in healthy mice. As far as the mechanistic insight is concerned, we focused on the attenuation of oxidative stress and the SAFE pathway. However, it remains unclear as to how our findings are linked to mitochondrial function and myocardial energy metabolism (26). Moreover, although this study dealt with the expression of several redox signaling molecules, such as NADPH oxidases and SOD, a number of other key controllers of mitochondrial reactive oxygen species emission, such as thioredoxin 2, were not explored (57). Finally, we acknowledge that defining the exact cell death pathways (apoptosis, necrosis, pyroptosis, necroptosis) that are affected by EMPA treatment is of major significance and requires future studies.

Materials and Methods

Animals
For the in vivo experiments, a total of 130 C57BL/6J male mice 12 weeks old (average weight 27.1 g) were used. The choice of the gender, the age and the strain of animals was based on the "Practical guidelines for rigor and reproducibility in preclinical and clinical studies on cardioprotection" (13) and our previous preclinical studies on I/R injury (4, 49). Mice were housed in a specific pathogen-free facility in a temperature-controlled environment (20°C-25°C) under a 12-h light/dark cycle, in a maximum number of six

per cage and received regular laboratory animal diet ad libitum. All animal procedures were in compliance with the Presidential Decree 56/2013 for the protection of the animals used for scientific purposes, in harmonization to the European Directive 2010/63; experimental protocols were approved by the competent Veterinary Service of the Prefecture of Athens (Protocol No. 2758/05-06-2018).
Surgical procedures on the animals and the interventions were performed in compliance with the guidelines "Practical guidelines for rigor and reproducibility in preclinical and clinical studies on cardioprotection" (13).

Pharmacological agents
The EMPA was isolated from 25 commercially available film-coated tablets (Jardiance F.C. Tab 25mg®; Boehringer Ingelheim, Germany), as previously reported (4). The pills were pulverized, and the powder was suspended in absolute Ethanol 99%. The suspension of the drug was then filtered through a pleated filter to remove the insoluble excipients. Afterward, the filtrate solution was centrifuged at 4000 g for 1Omin twice so that the remaining excipients could sediment. The supernatant was then vacuum vaporized, and EMPA was received as a crystal weight powder. The purity of the compound was verified via 1H-NMR spectroscopy as previously shown (4). The EMPA was diluted in water for injection and 5% DMSO to be administered to the animals and in pure DMSO for the in vitro assays.
Stattic, a commercially available STAT-3 inhibitor, was purchased from Sigma Aldrich (via Lab Supplies; P. Galanis & Co., Athens, Greece). Stattic was dissolved in pure DMSO for in vitro testing.
All reagents were purchased from Sigma Aldrich (via Lab Supplies; P. Galanis & Co.) and antibodies from Cell Signaling Technology (via Bioline; E. Demagkos & Co., Athens, Greece), unless otherwise stated.

Echocardiography
Echocardiography assessment was performed in the chronic cohort (n = 16, n = 8 per group), at baseline and at the end of the 6-week treatment with EMPA Echocardiographic analysis was performed in anesthetized mice with isoflurane (5% in 1 L/min oxygen for induction, and 1% for maintenance of anesthesia). Transthoracic echocardiography was performed by an experienced sonographer in a blinded manner with a high-frequency ultrasound imaging system (Vevo 2100; Visualsonics, Inc., Toronto, ON, Canada) equipped with an 18-38 MHz linear-array transducer (MS400). Heart rate, left ventricular end-diastole (LVEDD) and left ventricular end- systole diameter (LVESD), left ventricular posterior wall thickness at diastole and at systole, FS [FS% = (LVEDD - LVESD)/LVEDDx 100%], and left ventricular radius to left ventricular posterior wall thickness ratio were calculated (4, 20, 21).

Blood glucose levels
For the determination of blood glucose levels, mice were fasted for 8 h before the measurement. Blood sampling was performed by puncturing the tail vein vertically using a 23-gauge needle. The measurement of blood glucose was performed in three time points, at baseline, at the 21st day (in the middle of the protocol of EMPA treatment), and at the end of the treatment period. Blood glucose levels were measured by using the hand-held glucometer Accu-Chek Instant (Roche Diabetes Care GmbH) (4).

Arterial pressure monitoring
The arterial blood pressure was measured in the chronic cohort on awake mice (n = 16, n = 8 per group) at baseline and at the end of EMPA treatment with a noninvasive method by using the CODA Monitortail-cuff system (Kent Scientific Co., Torrington, CT). At first, the mice were placed for 10 min inside a heated chamber (34°C) and afterward in a restrainer over a heating pad. The tail cuff was positioned on the mouse tail, and the animals were allowed to acclimatize for 5 min. Then, 20 consecutive arterial pressure determination cycles were performed and the measurements were recorded on the CODA software (4). During our experiments, two animals exhibited signs of discomfort and therefore the animals were returned to the heated chamber and were re-examined 1 h later.

Murine model of ischemia-reperfusion injury
For the experiments of the myocardial infarction, mice were anesthetized with the use of an intraperitoneal combi- nation of ketamine (lO0 mg/kg), xylazine (20 mg/kg), and atropine (0.6 mg/kg). The anesthesia depth was monitored by the loss of the pedal reflex. The body temperature was maintained at 37°C throughout the surgical procedure with the use of a heating pad. A trachea! tube was placed via tracheotomy, and artificial respiration was set at a rate of 150 strokes per minute and with a tidal volume of 200 μL by using MiniVent Ventilator for Mice (Model 845; Harvard Apparatus). Then, the animals were positioned in left-lateral

recumbence and the chest was opened via left-sided thoracotomy. Afterward, the heart was visualized, the pericardium was incised, and the left anterior descending coronary was ligated ~ 3-4 mm distal to the origin of the artery under the left atrium by using a 6-0 silk suture. The heart was allowed to stabilize for 15 min. Ischemia was induced by tightening of the suture against a small piece of polyethylene tubing and was verified by checking for appearance of a paler color in the anterior wall of the left ventricle. At the end of the 30-min ischemic period, the ligature was released and allowed re- perfusion of the myocardium for 2 h, as previously described (4, 49).

Infarct size measurements

Infarct size measurement was employed to define the degree of myocardial injury from the ischemia and reperfusion insult in the two groups. Mice hearts were gently excised, and the aorta was cannulated and perfused with 5 mL of normal saline. Afterward, the suture was re-tightened and Evans Blue solution (2.5% in Water for injection) was slowly infused to delineate the ischemic from the normally perfused part of the myocardium. The hearts were frozen for 24 h at -20°C and were sliced into 1-2 mm sections. Tue slices were incubated with TTC solution (1% in phosphate-buffered saline [PBS] pH = 7.4) at 37°C for 20 min. Subsequently, the sections were emerged in formaldehyde overnight so that the infarct area is demarcated as a white area and the viable tissue stains red. The slices were photographed with a Cannon Powershot A620 Digital Camera (Canon, Tokyo, Japan) under the Zeiss 459300 microscope (Carl Zeiss Light Microscopy, Gottingen, Germany). For each heart, the overall size of each slice (All/A), the area-at-risk (R), and the infarct area (I) were determined by using ImageJ software and the percent- ages of RIA%, Salvage Index and 1/R % were calculated (4, 13, 19, 49).

Tissue sampling of the sham operated group

Mice were anesthetized and operated as described earlier. The 6-0 silk suture was ligated with the difference that the polyethylene tube was not placed and ischemia was not induced. Myocardial tissue samples were snap-frozen for the molecular mechanisms analyses (49).

Western blot analysis in myocardial tissue

Western blot analysis in myocardial tissue samples was performed as previously described (5, 53). Before the in- duction of ischemia, at the 10th minute of reperfusion or at the 2 h of reperfusion, tissue samples from the ischemic part of the myocardium were pulverized in liquid nitrogen and dry ice and were homogenized by using lysis solution (1% Triton Xl00, 20mMTris pH 7.4-7.6, 150mMNaCl, 50mM NaF, 1 mM EDTA, 1mM ethylene glycol tetraacetic acid, 1mM glycerolphosphatase, 1% sodium dodecyl sulfate [SDS], lO0mM phenylmethanesulfonyl fluoride, and 0.1% protease phosphatase inhibitor cocktail). Lowry method was employed for the determination of the protein content. An equal amount of protein was used to prepare the Western blot samples by mixing with Dave's buffer (4% SDS, 10% 2- mercaptoethanol, 20% glycerol, 0.004% bromophenyl blue, and 0.125 M Tris-HCl). The samples were boiled at 100°C for 10 min and stored at -80°C. The detection of the STAT-3 dimers was performed in tissue lysates prepared with suitable lysis buffer without SDS (NP-40 lysis buffer: 25mM Tris, 150mM NaCl, 1 mM EDTA, 1% NP-40, 5% glycerol, pH 7.4) supplemented with protease and phosphatase inhibitor tablets (Complete Mini, EDTA free Protease Inhibitor Cocktail; Roche Diagnostics GmbH and Pierce Phosphatase Inhibitor Mini Tablets; Thermo Scientific Product #A32757). The Western blot samples were mixed with Dave's buffer without 2-mercaproethanol and boiled at 90°C for 5 min. Tue samples were then separated by SDS-polyacrylamide gel electrophoresis 6-15% and transferred onto a polyvinylidene difluoride membrane. After blocking with 5% nonfat dry milk, membranes were incubated overnight at 4°C with the following primary antibodies: phospho-Akt (S473) (dilution 1:1000 Mouse, Cat. No E-AB-51038; Elabscience), Akt (dilution 1:1000, Mouse mAb #2920), phospho-STAT-3 (pSTAT-3; Y705) (dilution 1:1000, Mouse mAb #9138), tSTAT-3 (dilution 1:1000, Mouse mAb #9139), adenosine monophosphate-activated protein kinase a (p-AMPKα) (Tl72) (dilution 1:1000 Rabbit, NBl00-92711; Novus Biologicals), AMPKα (dilution 1:1000, Rabbit mAb #5831), glyceraldehyde-3-phosphate dehydrogenase (GAPDH) (dilution 1:4000, rabbit mAb #2118; Cell Signaling Technology), SOD2 (dilution 1:5000, rabbit mAb #13141; Cell Signaling Technology), VEGF (dilution 1:1000, mouse mAb, se Cat. No. sc-7269; purchased by Santa Cruz Biotechnology, Germany), and β-tubulin (dilution 1:1000 mouse mAb, Cat. No. sc-7963; purchased by Santa Cruz Biotechnology). Membranes were then incubated with secondary antibodies for 1-2 h at room temperature (Biorad goat anti-mouse and goat anti-rabbit horseradish peroxidase) and developed by using the GE Healthcare ECL Western

Blotting Detection Reagents (Thermo Scientific Technologies; Thermo Fisher Scientific, Inc., Waltham). Relative densitometry was determined, and the values for phosphoproteins were normalized to the values for total respective proteins (4, 49). The proteins P-tubulin or GAPDH were used as loading controls (49).

Measurement of myocardial MDA and PC content

The myocardial biopsies were snap-frozen in liquid nitrogen and stored at -80°C until the assay. The samples were pulverized and split in two parts before homogenization. For MDA measurement, the extraction was performed by using ice-cold 20 mM Tris-HCl buffer pH 7.4 whereas for PCs we used 0.1 M PBS pH= 6.7 in a 1:10 wt/volume ratio. Then, the samples were centrifuged at 3000 g for 10 min and 10,000 g for 15 min at 4°C and the supernatants were collected for the respective biochemical assays. The protein concentration of the supernatants was determined by the Lowry assay (DC protein assay; Bio-Rad, United Kingdom). The MDA con- centration was determined spectrophotometrically at 586 nm and expressed in μmol/mg protein (Oxford Biomedical Research Colorimetric Assay for lipid peroxidation) (5, 21). The PCs were measured spectrophotometrically at 360 nm and expressed in μmol/mg protein as previously described (5, 21). The measurements were performed on the plated reader Infinite 200 PRO series (Tecan).

Sample preparation for proteomic analysis

For proteomic analysis, the lysates that were prepared for Western blot analysis were used. Filter-aided sample preparation was performed according to a previously described method (33). Protein extracts (corresponding to 200μg total protein content for each sample) were mixed with 200μL of urea buffer (8 M urea in 0.1 MTris-HCl pH 8.5, UA buffer) in Amicon filter units (0.5 mL, 30 kDa MW cutoff) and were centrifuged at 14,000 g for 15 min. This step was repeated twice, and the flow-through was discarded form the collection tube. Then, 100μL of 0.05 M Iodoacetamide in UA buffer was added and mixed. The tubes were incubated for 20 min at room temperature in the dark. The filter units were centrifuged at 14,000 g for 10 min, washed with an equivalent volume of UA buffer, and centrifuged again. The flow through was discarded. Afterward, 100μL of ammonium bicarbonate buffer (50 mM NH4HCO3 pH 8, in ultrapure water) was added to the filter unit and centrifuged at 14,000 g for 10 min twice. Finally, the samples were trypsinized in a humidity container overnight at room temperature in the dark by using a solution of 50 mM NH4HCO3 pH 8, and trypsin to protein ratio 1:100 (w/w). The elution of peptides was recovered after centrifugation of the filter units at 14,000 g for 10 min. Centrifugation was repeated after another addition of 40μL 50 mM NH_4HCO_3 pH 8 into the filter units. Eluted peptides were lyophilized and stored at -80°C until use (35).

LC-MS analysis

All LC-MS/MS experiments were performed on the Dionex Ultimate 3000 UHPLC system coupled with the high- resolution nano-ESI Orbitrap-Elite mass spectrometer (Thermo Scientific) (34, 45). Each sample was reconstituted in 200μL loading solution composed of 0.1% v/v formic acid. A 5μL volume was injected and loaded on the Acclaim PepMap 100, 100μmx2 cm C18, 5μm, 100 A trapping column with the ulPickUp lnjection mode with the loading pump operating at flow rate 5μL/min. For the peptide separation, the Acclaim PepMap RSLC, 75μmx50cm, nano-Viper, C18, 2μm, and 100 A column retrofitted to a PicoTip emitter was used for multi-step gradient elution. Mobile phase (A) was composed of 0.1% formic acid and mobile phase (B) was composed of 100% acetonitrile, 0.1% formic acid. The peptides were eluted under a 240-min gradient from 2% (B) to 33% (B). Flow rate was 300 nL/min, and column temperature was set at 35°C. Gaseous phase transition of the separated peptides was achieved with positive ion electrospray ionization by applying a voltage of 2.5 kV. For every MS survey scan, the top 10 most abundant multiply charged precursor ions between m/z ratio 300 and 2200 and intensity threshold 500 counts were selected with FT mass resolution of 60,000 and subjected to higher- energy collisional dissociation fragmentation. Tandem mass spectra were acquired with an FT resolution of 15,000. Normalized collision energy was set to 33, and already targeted precursors were dynamically excluded for further isolation and activation for 45 s with 5 ppm mass tolerance (45, 58).

MS data processing and quantification

Raw files were analyzed with Proteome Discoverer 1.4 software package (Thermo Finnigan), using the Sequest search engine and the Uniprot mouse (Mus musculus) reviewed database, downloaded on November 22, 2017, including 16,935 entries. The search was performed by using carbamidomethylation of cysteine as static and oxidation of methionine as dynamic modifications. Two missed cleavage sites, a precursor mass

tolerance of 10 ppm, and fragment mass tolerance of 0.05 Da were allowed. False discovery rate (FDR) validation was based on q value: target FDR: 0.01. (45).
Quantification was performed at the peptide level by employing a clustering approach as previously described (40, 58). Label-free quantification was performed by utilizing the precursor area values of each sample as defined by the Proteome Discoverer 1.4 software package. Samples were analyzed individually (not pooled) and assigned to distinct groups. For a small number of peptide sequences where no peptide precursor area could be retrieved (although the peptides were identified), the missing values were replaced by zero. If a peptide was not identified in a particular sample, the missing values were replaced by zero. For the quantitation- statistical analysis, only the peptides that were present in at least 75% of the samples in at least one group were further considered. The precursor area values were subjected to the following normalization method within each sample before quantification analysis: normalized peak area=(peptide peak area/sum of peptides peak area)x106. Protein expression values were calculated as the sum of all the normalized peptide areas that were assigned for a given protein. p-Value ≤ 0.05 was considered statistically significant. Visualization of the proteomics findings in the form of the heat map was performed by using the ClusterVis web server(44). The gene names used in the heatmap, in Supplementary Tables S3 and S4 and wherever else indicated were updated on September 2019 based on UniProt database.

Functional analysis
Functional analysis was performed with the WebGestat (65) Analysis web interface by using the default settings. Ontologies were retrieved from Wikipathways database (updated on 2017), and only statistically significant pathways (Benjamini-Hochberg corrected p-value ≤ 0.05, two-sided hypergeometric test) were taken into account. For the remaining parameters, default settings were used.

Confocal microscopy
Myocardial cryosections were fixed with 4% paraformaldehyde, permeabilized with 0.25% TritonX in PBS, and blocked with 3% bovine serum alburnin-0.01% Tween- 80 (Cat. No. A8806; Sigma Aldrich) in PBS. Subsequently, samples were incubated with pSTAT-3(Y703) (Mouse mAb, #4113S; Cell Signaling), CD31 (Rabbit pAb, # ab28364; Abcam), and VEGFR2 (Rabbit pAb, #ab39256; Abcam). Primary antibodies were incubated with the specimens overnight, washed off with PBS and subsequently anti-rabbit/ Alexa-Fluor 647 (Donkey, # abl50079; Abcam) and anti-mouse/Alexa-Fluor 594 (Donkey, # abl50120; Abcam) conjugated secondary antibodies were used. After washing trice in PBS, specimens were treated with VECTASHIELD antifade mounting medium with 4',6-diamidino-2- phenylindole (DAPI) for DNA staining (Cat. No. H-1200; Vector) and visualized in a confocal laser-scanning microscope (Leica confocal microscope, 40 x, oil immersion objective). Z stacks of the cells were obtained, and 3D images were generated by using Fiji-ImageJ software2 (21). The integrated fluorescence density of each 3D image for each channel was measured by using the same software.

Real-time PCR
For isolation of RNA, snap-frozen murine hearts were pulverized and extracted by the standardized Trizol protocol. The RT-PCR was performed with the CFX96 Real-Time PCR Detection System (Bio-Rad, Munich, Germany). Isolated RNA was reverse-transcribed to cDNA by using high-capacity cDNA reverse transcription kit (Takara). The following primer pairs were designed (Primer-Blast, NCBI, NIH) and used to detect mRNA expression; Nos3, Vegfα, Vegfβ, Vegfr2, Nos2, Sod2, and Nox2 (Eurofins Genomics AT, GmbH) were analyzed by the standardized SYBR®Green method (Kapa Biosystems) according to the manufacturer's instructions (32). The comparative delta CT method was used for relative mRNA quantification. We normalized gene expression to the endogenous control (TBP mRNA), and the expression of the target gene mRNA of each sample was expressed relative to that of the control (56).

Gene (M. Musculus)	**Primer (5'-3')**	**Product length**
Nos3	Forward GGCTGTAGCCCTATTTCACCT Reverse ATTGTTGGGCTTTGCTTCACT	83
Nos2	Forward AGGCAATCTTCGTTCAGCCA Reverse TAGCCCGCATAGCGTATCAG	99
Nox2	Forward AAGTTCGCTGGAAACCCTCC	88

	Reverse GCCAAAACCGAACCAACCTC	
Sod2	Forward CTGAAGTTCAATGGTGGGGG Reverse CAGCAACTCTCCTTTGGGTTC	93
Gadph	Forward CCCAGCTTAGGTTCATCAGGT Reverse GCCAAATCCGTTCACACCG	87
Vegfβ	Forward AGCCAGACAGGGTTGCCAT Reverse TGGATGATGTCAGCTGGGGAG	100
Vegfα	Forward CTGGACCCTGGCTTTACTGC Reverse ACTTGATCACTTCATGGGACTTCT	98

HMECs culture
The HMECs were obtained from the American Type Culture Collection (ATCC, Manassas, V A). The HMECs were grown in MCDB 131 Medium supplemented with 10% fetal bovine serum (FBS) and 1% (v/v) streptomycin/ penicillin at 37°C and 5% CO_2. At 80% confluence, the cells were seeded in a 96-well plate or in a 6-well plate at 2.5 x103 per well or 5 x104 per well and left in culture for 24 h to perform Cell Viability Test and ROS Detection Assay, respectively.

Hypoxia/reoxygenation protocol
For in vitro H/R experiments, HMEC were serum-starved (FBS 2%) for 24 h and treated with EMPA (500 nM) for 24 h. Then, cells were exposed to hypoxia (5% CO_2 and 94% N_2) for 3 h (in the presence of EMPA) and subsequently reoxygenated (21% O_2 and 5% CO_2) for 1 h. During reoxygenation, the cells were exposed to STAT-3 inhibitor, Stattic (500 nM).

MTTassay
At the end of the H/R protocol, cell viability was assessed by using the MTT kit (10 µL/well; Sigma, St. Louis, MO) as indicated by the manufactory protocol. Briefly, after 2h of incubation at 37°C, DMSO (Sigma) was added. Each experiment was performed three times (16 wells/each experimental condition). The plates were read at 570 nm to obtain optical density values.

ROS detection assay
At the end of the H/R protocol, ROS generation was evaluated by using the Oxidative Stress Kit (Muse® Oxidative Stress Kit; Millipore). Each experiment was performed three times.

Statistical analysis
Statistical analysis was performed by using the GraphPad Prism 7 software (Graph Pad Software, Inc.). All the results were plotted in graphs as mean ± standard error of the mean values. For animal studies, tissue experiments, densitometric analysis for Western blots, PCR, and cell viability assay on normoxia comparisons of numeric variables between the two groups were conducted by using an unpaired two-tailed Student's t-test. Echocardiography and blood pressure data originating from different time points belonging to the same group were analyzed by using a paired two-tailed Student's t-test. A calculated $p < 0.05$ was considered statistically significant. For PCA, SIMCA P+ 11.5 was used.
Data on STAT-3 phosphorylation and expression under nonreducing conditions, cell viability assay, and ROS assay were analyzed by using one-way analysis of variance, followed by Tukey's multiple-comparison test. Glucose levels and body weights were analyzed by using paired two-way analysis of variance (comparing the means among groups and using Bonferroni as a post hoc test for multiple comparisons) as required. The cut-off for statistical significance was set at $p < 0.05$ (*$p < 0.05$, **$p < 0.01$, ***$p < 0.001$, ****$p < 0.0001$).

Author Disclosure Statement
No competing financial interests exist.

Funding Information
This work has been supported by the EU-CARDIOPROTECTION COST-Action (CA16225).

References

1. Abdurrachim D, Manders E, Nicolay K, Mayoux E, and Prompers JJ. Single dose of empagliflozin increases in vivo cardiac energy status in diabetic db/db mice. Cardiovasc Res 114: 1843-1844, 2018.
2. Abhinand CS, Raju R, Soumya SJ, Arya PS, and Sudhakaran PR. VEGF-ANEGFR2 signaling network in endothelial cells relevant to angiogenesis. J Celi Commun Signal 10: 347-354, 2016.
3. Andreadou I, Bell RM, B!2Stker HE, and Zuurbier CJ. SGLT2 inhibitors reduce infarct size in reperfused ischemie heart and improve cardiac function during ischemie epi- sodes in preclinical models. Biochim Biophys Acta 1866: 165770, 2020.
4. Andreadou I, Efentakis P, Balafas E, Togliatto G, Davos CH, Varela A, Dimitriou CA, Nikolaou P-E, Maratou E, Lambadiari V, Ikonomidis I, Kostomitsopoulos N, Brizzi MF, Dimitriadis G, and Iliodromitis EK. Empagliflozin limits myocardial infarction in vivo and cell death in vitro: role of STAT3, mitochondria, and redox aspects. Front Physiol 8: 1077, 2017.
5. Andreadou I, Farmakis D, Prokovas E, Sigala F, Zoga A, Spyridaki K, Papalois A, Papapetropoulos A, Anastasiou- Nana M, Kremastinos DT, and Iliodromitis EK. Short-term statin administration in hypercholesterolaemic rabbits resistant to postconditioning: effects on infarct size, endo- thelial nitric oxide synthase, and nitro-oxidative stress. Cardiovasc Res 94: 501-509, 2012.
6. Baartscheer A, Schumacher CA, Wiist RCI, Fiolet JWT, Stienen GJM, Coronel R, and Zuurbier CJ. Empagliflozin decreases myocardial cytoplasmic Na+ through inhibition of the cardiac Na+>/H+ exchanger in rats and rabbits. Diabetologia 60: 568-573, 2017.
7. Bader AM, Brodarac A, Klose K, Bieback K, Choi Y-H, Kurtz A, and Stamm C. Mechanisms of paracrine cardio- protection by cord blood mesenchymal stromal cells. Eur J Cardiothorac Surg 45: 983-992, 2014.
8. Barlow HR and Cleaver O. Building blood vessels-one Rho GTPase at a time. Cells 8: E545, 2019.
9. Bartoli M, Platt D, Lemtalsi T, Gu X, Brooks SE, Marrero MB, and Caldwell RB. VEGF differentially activates STAT3 in microvascular endothelial cells. FASEB J 17: 1562-1564, 2003.
10. Boengler K, Buechert A, Heinen Y, Roeskes C, Hilfiker- Kleiner D, Heusch G, and Schulz R. Cardioprotection by ischemie postconditioning is lost in aged and STAT3- deficient mice. Circ Res 102: 131-135, 2008.
11. Boengler K, Hilfiker-Kleiner D, Heusch G, and Schulz R. Inhibition of permeability transition pore opening by mi- tochondrial STAT3 and its role in myocardial ischemia/ reperfusion. Basic Res Cardiol 105: 771-785, 2010.
12. Bolli R, Dawn B, and Xuan Y-T. Role of the JAK-STAT pathway in protection against myocardial ischemia/ reperfusion injury. Trends Cardiovasc Med 13: 72-79, 2003.
13. B!2Stker HE, Hausenloy D, Andreadou I, Antonucci S, Boengler K, Davidson SM, Deshwal S, Devaux Y, Di Lisa F, Di Sante M, Efentakis P, Femminò S, Garcfa-Dorado D, Giricz Z, lbanez B, Iliodromitis E, Kaludercic N, Kleinbongard P, Neuhauser M, Ovize M, Pagliaro P, Rahbek-Schmidt M, Ruiz-Meana M, Schliiter K-D, Schulz R, Skyschally A, Wilder C, Yellon DM, Ferdinandy P, and Heusch G. Practical guidelines for rigor and reproducibility in preclinical and clinical studies on cardioprotection. Basic Res Cardiol 113: 39, 2018.
14. Chen Z and Han ZC. STAT3: a critica! transcription acti- vator in angiogenesis. Med Res Rev 28: 185-200, 2008.
15. Chu C, Lu Y-P, Yin L, and Hocher B. The SGLT2 inhibitor empagliflozin might be a new approach for the prevention of acute kidney injury. Kidney Blood Press Res 44: 149- 157, 2019.
16. Connelly KA, Zhang Y, Visram A, Advani A, Batchu SN, Desjardins J-F, Thai K, and Gilbert RE. Empagliflozin improves diastolic function in a nondiabetic rodent model of heart failure with preserved ejection fraction. J Am Coll Cardiol Basic Trans Sci 4: 27-37, 2019.
17. Davidson SM, Ferdinandy P, Andreadou I, B!2Stker HE, Heusch G, lbaiiez B, Ovize M, Schulz R, Yellon DM, Hausenloy DJ, Garcia-Dorado D; Action (CA16225) on Behalf of the EUCC. Multitarget strategies to reduce myocardial ischemia/reperfusion injury: JACC review topic of the week. J Am Coll Cardiol 73: 89-99, 2019.

18. Dhalla NS, Elmoselhi AB, Hata T, and Makino N. Status of myocardial antioxidants in ischemia-reperfusion injury. Cardiovasc Res 47: 446--456, 2000.
19. Efentakis P, Andreadou I, Bibli S-1, Vasileiou S, Dagres N, Zoga A, Lougiakis N, Kremastinos DT, and Iliodromitis EK. Ranolazine triggers pharmacological preconditioning and postconditioning in anesthetized rabbits through acti- vation of RISK pathway. Eur J Pharmacol 789: 431-438, 2016.
20. Efentakis P, Kremastiotis G, Varela A, Nikolaou P-E, Papanagnou E-D, Davos CH, Tsoumani M, Agrogiannis G, Konstantinidou A, Kastritis E, Kanaki Z, Iliodromitis EK, Klinakis A, Dimopoulos MA, Trougakos IP, Andreadou I, and Terpos E. Molecular mechanisms of Carfilzomib- induced cardiotoxicity in mice and the emerging cardio- protective role of Metformin. Blood 133: 710-723, 2019.
21. Efentakis P, Varela A, Chavdoula E, Sigala F, Sanoudou D,
Tenta R, Gioti K, Kostomitsopoulos N, Papapetropoulos A, Tasouli A, Farmakis D, Davos CH, Klinakis A, Suter T, Cokkinos DV, Iliodromitis EK, Wenzel P, and Andreadou
I. Levosimendan prevents doxombicin-induced cardio- toxicity in time- and dose dependent manner: Implications for inotropy. Cardiovasc Res 116: 576-591, 2020.
22. Egea J, Fabregat I, Frapart YM, Ghezzi P, Gorlach A, Kietzmann T, Kubaichuk K, Knaus UG, Lopez MG, Olaso- Gonzalez G, Petry A, Schulz R, Vina J, Winyard P, Abbas K, Ademowo OS, Afonso CB, Andreadou I, Antelmann H, Antunes F, Aslan M, Bachschmid MM, Barbosa RM, Belousov V, Bemdt C, Bemlohr D, Bertran E, Bindoli A, Bottari SP, Brito PM, Carrara G, Casas Al, Chatzi A, Chondrogianni N, Conrad M, Cooke MS, Costa JG, Cuadrado A, My-Chan Dang P, De Smet B, Debelec- Butuner B, Dias IHK, Dunn JD, Edson AJ, El Assar M, El- Benna J, Ferdinandy P, Fernandes AS, Fladmark KE, Forstermann U, Giniatullin R, Giricz Z, Gorbe A, Griffiths H, Hampl V, Hanf A, Herget J, Hernansanz-Agustfo P, Hillion M, Huang J, Ilikay S, Jansen-Diirr P, Jaquet V, Joles JA, Kalyanaraman B, Karninskyy D, Karbaschi M, Kleanthous M, Klotz L-O, Korac B, Korkmaz KS, Koziel R, Kracun D, Krause K-H, Ki'en V, Krieg T, Laranjinha J, Lazou A, Li H, Martfnez-Ruiz A, Matsui R, McBean GJ, Meredith SP, Messens J, Miguel V, Mikhed Y, Milisav I, Milković L, Miranda-Vizuete A, Mojović M, Monsalve M, Mouthuy P-A, Mulvey J, Miinzel T, Muzykantov V, Nguyen ITN, Oelze M, Oliveira NG, Palmeira CM, Papaevgeniou N, Paviéevié A, Pedre B, Peyrot F, Phylac- tides M, Pircalabioru GG, Pitt AR, Poulsen HE, Prieto I, Rigobello MP, Robledinos-Ant6n N, Rodriguez-Mafias L, Rolo AP, Rousset F, Ruskovska T, Saraiva N, Sasson S, Schroder K, Semen K, Seredenina T, Shakirzyanova A, Srnith GL, Soldati T, Sousa BC, Spickett CM, Stancic A, Stasia MJ, Steinbrenner H, Stepanié V, Steven S, Tokatlidis K, Tuncay E, Turan B, Ursini F, Vacek J, Vajnerova O, Valentova K, Van Breusegem F, Varisli L, Veal EA, Yalçm AS, Yelisyeyeva O, Zarkovié N, Zatloukalova M, Zielonka J, Touyz RM, Papapetropoulos A, Grone T, Lamas S, Schrnidt HHHW, Di Lisa F, and Daiber A. European contribution to the study ofROS: a summary ofthe findings and prospects for the future from the COST action BM1203 (EU-ROS). Redox Biol 13: 94-162, 2017.
23. Ferdinand KC, Izzo JL, Lee J, Meng L, George J, Salsali A, and Seman L. Antihyperglycernic and blood pressure ef- fects ofempagliflozin in black patients with type 2 diabetes mellitus and hypertension. Circulation 139: 2098-2109,
2019.
24. Ferrannini E. Sodium-glucose co-transporters and their inhibition: clinical physiology. Celi Metab 26: 27-38, 2017.
25. Frampton JE. Empagliflozin: a review in type 2 diabetes.
Drugs 78: 1037-1048, 2018.
26. Garcfa-Ropero A, Vargas-Delgado AP, Santos-Gallego CG, and Badimon JJ. Inhibition of sodium glucose co- transporters improves cardiac performance. lnt J Mol Sci 20: E3289, 2019.
27. Habibi J, Aroor AR, Sowers JR, Jia G, Hayden MR, Garro M, Barron B, Mayoux E, Rector RS, Whaley-Connell A, and DeMarco VG. Sodium glucose transporter 2 (SGLT2) inhibition with empagliflozin improves cardiac diastolic function in a female rodent model ofdiabetes. Cardiovasc Diabetol 16: 9, 2017.
28. Hausenloy DJ, Lecour S, and Yellon DM. Reperfusion injury salvage kinase and survivor activating factor en- hancement prosurvival signaling pathways in ischemie postconditioning: two sides of the same coin. Antioxid Redox Signa/ 14: 893-907, 2011.
29. Hawley SA, Ford RJ, Smith BK, Gowans GJ, Mancini SJ, Pitt RD, Day EA, Salt IP, Steinberg GR, and Hardie DG. The Na+/glucose cotransporter inhibitor canagliflozin ac- tivates AMPK by inhibiting rnitochondrial function and increasing cellular AMP levels. Diabetes 65: 2784-2794, 2016.
30. Heusch G. Molecular basis of cardioprotection. Circ Res
116: 674--699, 2015.
31. lborra-Egea O, Santiago-Vacas E, Yurista SR, Lup6n J, Packer M, Heymans S, Zannad F, Butler J,

Pascual-Figal D, Lax A, Nuiiez J, Boer RA de, and Bayés-Genis A. Un- raveling the molecular mechanism of action of empagli- tlozin in heart failure with reduced ejection fraction with or without diabetes. J Am Coli Cardiol Basic Trans Sci 4: 831-840, 2019.
31a. Jespersen NR, Lassen TR, Hjortbak MV, St!,'Jttrup NB and B!,'Jtker HE. Sodium glucose transporter 2 (SGLT2) inhi- bition does not protect the myocardium from acute ische- mie reperfusion injury but modulates postischemic mitochondrial function. Cardiovasc Pharmacol 6: 210,
2017.
32. Kossmann S, Lagrange J, Jlickel S, Jurk K, Ehlken M, Schonfelder T, Weihert Y, Knorr M, Brandt M, Xia N, Li H, Daiber A, Oelze M, Reinhardt C, Lackner K, Gruber A, Monia B, Karbach SH, Walter U, Ruggeri ZM, Renné T, Ruf W, Miinzel T, and Wenzel P. Platelet-localized FXI promotes a vascular coagulation-inflammatory circuit in arterial hypertension. Sci Transi Med 9: eaah4923, 2017.
33. Latosinska A, Makridakis M, Frantzi M, Borràs DM, Janssen B, Mullen W, Zoidakis J, Merseburger AS, Jankowski V, Mischak H, and Vlahou A. Integrative analysis of extracellular and intracellular bladder cancer cell line proteome with transcriptome: improving coverage and validity of-ornics findings. Sci Rep 6: 25619, 2016.
34. Latosinska A, Mokou M, Makridakis M, Mullen W, Zoidakis J, Lygirou V, Frantzi M, Katafigiotis I, Stravo- dimos K, Hupe MC, Dobrzynski M, Kolch W, Merseburger AS, Mischak H, Roubelakis MG, and Vlahou A. Pro- teornics analysis of bladder cancer invasion: targeting EIF3D for therapeutic intervention. Oncotarget 8: 69435- 69455, 2017.
35. Latosinska A, Vougas K, Makridakis M, Klein J, Mullen W, Abbas M, Stravodimos K, Katafigiotis I, Merseburger AS, Zoidakis J, Mischak H, Vlahou A, and Jankowski V. Comparative analysis of label-free and 8-Plex iTRAQ ap- proach for quantitative tissue proteornic analysis. PLoS One 10: e0137048, 2015.
36. Lee PC, Ganguly S, and Goh S-Y. Weight loss associated with sodium-glucose cotransporter-2 inhibition: a review of evidence and underlying mechanisms. Obes Rev 19: 1630---1641, 2018.
37. Lee T-M, Chang N-C, and Lin S-Z. Dapagliflozin, a se- lective SGLT2 Inhibitor, attenuated cardiac fibrosis by regulating the macrophage polarization via STAT3 signal- ing in infarcted rat hearts. Free Radic Biol Med 104: 298- 310, 2017.
38. Lim VG, Bell RM, Arjun S, Kolatsi-Joannou M, Long DA, and Yellon DM. SGLT2 inhibitor, canagliflozin, attenuates myocardial infarction in the diabetic and nondiabetic heart. JACC Basic Transi Sci 4: 15-26, 2019.
39. Lubec G and Afjehi-Sadat L. Lirnitations and pitfalls in protein identification by mass spectrometry. Chem Rev l 07: 3568-3584, 2007.
40. Lygirou V, Latosinska A, Makridakis M, Mullen W, Delles C, Schanstra JP, Zoidakis J, Pieske B, Mischak H, and Vlahou A. Plasma proteomic analysis reveals altered pro- tein abundances in cardiovascular disease. J Transi Med 16: 104, 2018.
41. Mancini SJ, Boyd D, Katwan OJ, Strembitska A, Almab- rouk TA, Kennedy S, Palmer TM, and Salt IP. Canagli- flozin inhibits interleukin-1,B-stimulated cytokine and chemokine secretion in vascular endothelial cells by AMP-activated protein kinase-dependent and -independent mechanisms. Sci Rep 8: 5276, 2018.
42. McMurray JN, Salomon SD, Inzucchi SE, Kiaber L, Kosiborod MN, Martinez FA, Ponikowski P, Sabatine MS, Anand IS, Belohlavek J, Bohm M, Chiang C-E, Chopra VK, de Boer RA, Desai AS, Diez M, Drozdz J, Dukat A, Ge J, Howlett JG, Katova T, Kitakaze M, Ljungman CEA, Merkely B, Nicolau JC, O'Meara E, Petrie MC, Vinh PN, Schou M, Tereshchenko S, Verma S, Held C, DeMets DL, Docherty KF, Jhund PS, Bengtsson O, Sjostrand M, Lang- kilde A-M; DAPA-HF Trial Committees and Investigators. Dapagliflozin in patients with heart failure and reduced ejection fraction. N Engl J Med 381: 1995-2008, 2019.
43. Meng X, Brown JM, Ao L, Shames BD, Banerjee A, and Harken AH. Reduction of infarct size in the rat heart by LPS preconditioning is associated with expression of an- giogenic growth factors and increased capillary density. Shock 12: 25-31, 1999.
44. Metsalu T and Vilo J. ClustVis: a web tool for visualizing clustering of multivariate data using principal component analysis and heatmap. Nucleic Acids Res 43: W566-W570, 2015.
45. Mokou M, Klein J, Makridakis M, Bitsika V, Bascands J-L, Saulnier-Blache JS, Mullen W, Sacherer M, Zoidakis J, Pieske B, Mischak H, Roubelakis MG, Schanstra JP, and Vlahou A. Proteomics based identification of KDM5 his- tone demethylases associated with cardiovascular disease. EBioMedicine 41: 91-104, 2019.
46. Motherwell JM, Anderson CR, and Murfee WL. Endothelial cell phenotypes are maintained during

angiogenesis in cul- tured microvascular networks. Sci Rep 8: 1-11, 2018.
47. Neal B, Perkovic V, Mahaffey KW, de Zeeuw D, Fulcher G, Erondu N, Shaw W, Law G, Desai M, and Matthews DR. Canagliflozin and cardiovascular and renal events in type 2 diabetes. N Engl J Med 377: 644--657, 2017.
48. Neuen BL, Ohkuma T, Neal B, Matthews DR, de Zeeuw D, Mahaffey KW, Fulcher G, Desai M, Li Q, Deng H, Rosenthal N, Jardine MJ, Bakris G, and Perkovic V. Cardiovascular and renal outcomes with canagliflozin ac- cording to baseline kidney function. Circulation 138: 1537-1550, 2018.
49. Nikolaou P-E, Boengler K, Efentakis P, Vouvogianno- poulou K, Zoga A, Gaboriaud-Kolar N, Myrianthopoulos
V, Alexakos P, Kostomitsopoulos N, Rerras I, Tsantili- Kakoulidou A, Skaltsounis AL, Papapetropoulos A, Ilio- dromitis EK, Schulz R, and Andreadou I. Investigating and re-evaluating the role of glycogen synthase kinase 3 beta kinase as a molecular target for cardioprotection by using novel pharmacological inhibitors. Cardiovasc Res 115: 1228-1243, 2019.
50. This reference has been deleted.
51. Oelze M, Kroller-Schon S, Welschof P, Jansen T, Hausding M, Mikhed Y, Stamm P, Mader M, ZinBius E, Agdauletova S, Gottschlich A, Steven S, Schulz E, Bottari SP, Mayoux E, Mtinzel T, and Daiber A. The sodium-glucose co- transporter 2 inhibitor empagliflozin improves diabetes- induced vascular dysfunction in the streptozotocin diabetes rat model by interfering with oxidative stress and gluco- toxicity. PLoS One 9: e112394, 2014.
52. Oliva RV and Bakris GL. Blood pressure effects ofsodium- glucose co-transport 2 (SGLT2) inhibitors. J Am Soc Hypertens 8: 330-339, 2014.
53. Penna C, Perrelli M-G, and Pagliaro P. Mitochondrial pathways, permeability transition pore, and redox signaling in cardioprotection: therapeutic implications. Antioxid Redox Signa[18: 556--599, 2012.
54. Prasad V, Lorenz JN, Miller ML, Vairamani K, Nieman ML, Wang Y, and Shull GE. Loss ofNHEl activity leads to reduced oxidative stress in heart and mitigates high-fat diet-induced myocardial stress. J Mol Celi Cardiol 65: 33--42, 2013.
55. Sayour AA, Korkmaz-lcoz S, Loganathan S, Ruppert M, Sayour VN, Olah A, Benke K, Brune M, Benko R, Horvath EM, Karck M, Merkely B, Radovits T, and Szab6 G. Acute canagliflozin treatment protects against in vivo myocardial ischemia-reperfusion injury in non-diabetic male rats and enhances endothelium-dependent vasorelaxation. J Transi Med 17: 127, 2019.
56. Schiller R, Efentakis P, Wild J, Lagrange J, Garlapati V, Molitor M, Kossmann S, Oelze M, Stamm P, Li H, Schli.fer K, Milnzel T, Daiber A, Waisman A, Wenzel P, and Karbach SH. T Cell-derived IL-17A induces vascular dysfunction via perivascular fibrosis formation and dysre- gulation of • NO/cGMP signaling. Oxid Med Celi Longev 2019: 6721531, 2019.
57. Stanley BA, Sivakumaran V, Shi S, McDonald I, Lloyd D, Watson WH, Aon MA, and Paolocci N. Thioredoxin reductase-2 is essential for keeping low levels of H(2)O(2) emission from isolated heart mitochondria. J Biol Chem 286: 33669-33677, 2011.
58. Stroggilos R, Mokou M, Latosinska A, Makridakis M, Lygirou V, Mavrogeorgis E, Drekolias D, Frantzi M, Mullen W, Fragkoulis C, Stasinopoulos K, Papadopoulos G, Stathouros G, Lazaris AC, Makrythanasis P, Ntoumas K, Mischak H, Zoidakis J, and Vlahou A. Proteome-based classification of Nonmuscle Invasive Bladder Cancer. Int J Cancer 146: 281-294, 2020.
59. Tahara A, Takasu T, Yokono M, Imamura M, and Kurosaki
E. Characterization and comparison of sodium-glucose cotransporter 2 inhibitors in pharmacokinetics, pharmaco- dynamics, and pharmacologic effects. J Pharmacol Sci 130: 159-169, 2016.
60. Terami N, Ogawa D, Tachibana H, Hatanaka T, Wada J, Nakatsuka A, Eguchi J, Horiguchi CS, Nishii N, Yamada H, Takei K, and Makino H. Long-term treatment with the sodium glucose cotransporter 2 inhibitor, dapagliflozin, ameliorates glucose homeostasis and diabetic nephropathy in db/db mice. PLoS One 9: e100777, 2014.
61. Timmis A, Townsend N, Gale C, Grobbee R, Maniadakis N, Flather M, Wilkins E, Wright L, Vos R, Bax J, Blum M, Pinto F, and Vardas P. European Society of Cardiology: cardiovascular disease statistics 2017. Eur Heart J 39: 508-
579, 2018.
62. Uthman L, Nederlof R, Eerbeek O, Baartscheer A, Schu- macher C, Buchholtz N, Hollmann MW, Coronel R, Weber NC, and Zuurbier CJ. Delayed ischaemic contracture onset by empagliflozin associates with NHEl inhibition and is dependent on insulin in isolated mouse hearts. Cardiovasc Res 115: 1533-1545, 2019.

63. Van AS, Balteau M, Ginion A, Ferté L, Battault S, Ravenstein CM, Balligand JL, Daskalopoulos EP, Gilon P, Despa F, Despa S, Vanoverschelde JL, Horman S, Koepsell H, Berry G, Hue L, Bertrand L, and Beauloye C. Sodium- myoinositol cotransporter-1, SMITl, mediates the produc- tion of reactive oxygen species induced by hyperglycemia in the heart. Sci Rep 7: 41166, 2017.
64. Wang J, Duncan D, Shi Z, and Zhang B. WEB-based GEne SeT AnaLysis Toolkit (WebGestalt): update 2013. Nucleic Acids Res 41: W77-W83, 2013.
65. Wang J, Vasaikar S, Shi Z, Greer M, and Zhang B. Web- Gestalt 2017: a more comprehensive, powerful, flexible and interactive gene set enrichment analysis toolkit. Nucleic Acids Res 45: W130--W137, 2017.
66. Wiviott SD, Raz I, Bonaca MP, Mosenzon O, Kato ET, Cahn A, Silverman MG, Zelniker TA, Kuder JF, Murphy SA, Bhatt DL, Leiter LA, McGuire DK, Wilding JPH, Ruff CT, Gause-Nilsson IAM, Fredriksson M, Johansson PA, Langkilde A-M, Sabatine MS; DECLARE-TIMI 58 In- vestigators. Dapagliflozin and cardiovascular outcomes in type 2 diabetes. N Engl J Med 380: 347-357, 2019.
67. Ye Y, Jia X, Bajaj M, and Birnbaum Y. Dapagliflozin attenuates Na+/H+ exchanger-1 in cardiofibroblasts via AMPK activation. Cardiovasc Drugs Ther 32: 553-558, 2018.
68. Yurista SR, Silljé HHW, Oberdorf-Maass SU, Schouten E-M, Pavez Giani MG, Hillebrands J-L, van Goor H, van Veldhuisen DJ, de Boer RA, and Westenbrink BD. Sodium- glucose co-transporter 2 inhibition with empagliflozin improves cardiac function in non-diabetic rats with left ventricular dysfunction after myocardial infarction. Eur J Heart Fail 21: 862-873, 2019.
69. Zgheib C, Kurdi M, Zouein FA, Gunter BW, Stanley BA, Zgheib J, Romero DG, King SB, Paolocci N, and Booz GW. Acyloxy nitroso compounds inhibit LIF signaling in endo- thelial cells and cardiac myocytes: evidence that STAT3 signaling is redox-sensitive. PLoS One 7: e43313, 2012.
70. Zgheib C, Zouein FA, Kurdi M, and Booz GW. Differential STAT3 signaling in the heart. JAKSTAT 1: 101-110, 2012.
71. Zhang Y, Nakano D, Guan Y, Hitorni H Uemura A Masaki T, Kobara H, Sugaya T, and Nishiyama A. sodium-glucose cotransporter 2 inhibitor attenuates renal capillary injury and fibrosis by a vascular endothelial growth factor---dependent pathway after renal injury in rnice. Kidney Int 94: 524--535, 2018.
72. Zhou H, Wang S, Zhu P, Hu S, Chen Y, and Ren J. Empagliflozin rescues diabetic myocardial microvascular injury via AMPK-mediated inhibition of rnitochondrial fission. Redox Biol 15: 335-346, 2018.
73. Zinman B, Wanner C, Lachin JM, Fitchett D, Bluhmki E, Hantel S, Mattheus M, Devins T, Johansen OE, Woerle HJ, Broedl UC, and Inzucchi SE. Empagliflozin, cardiovascular outcomes, and mortality in type 2 diabetes. N Engl J Med 373: 2117-2128, 2015.
74. Zouein FA, Altara R, Chen Q, Lesnefsky EJ, Kurdi M, and Booz GW. Pivotal Importance of STAT3 in protecting the heart from acute and chronic stress: new advancement and unresolved issues. Front Cardiovasc Med 2: 36, 2015.

TABLE 1.

Arterial blood pressure measurements at baseline and after 6 weeks of empagliflozin administration using the tail-cuff system

Blood pressure	***Control, mmHg, n=8***	***EMPA, mmHg, n=8***	***p***
Mean BP baseline	108.3±3.6	113.5±2.3	0.2436
Mean BP 6 weeks	92.4±4.9	98.1±6.1	0.4783
Systolic BP baseline	126.7±3.9	135.1±2.0	0.0772
Systolic BP 6 weeks	111.8±5.8	117.5±7.1	0.5460
Diastolic BP baseline	99.5±3.6	103.0±2.5	0.4351
Diastolic BP 6 weeks	83.0±4.5	88.9±5.7	0.4292

Unpaired t-test was employed for comparison between the two groups, and paired t-test was use for the comparison of the two different time point measurements of the same group. The results demonstrate no significant change between the groups (n = 8 per group, p=NS). Data are presented as mean±SEM. BP, blood pressure; EMPA, empagliflozin; SEM, standard error of the mean.

TABLE 2.

Echocardiographic assessment of cardiac function at 6 weeks between empagliflozin-treated mice and the control group demonstrated a slightly reduced heart rate in the empagliflozin group

6 Weeks	***Contro/, n=8***	***EMPA, n=8***	***p***
HR, beats/min	573.87 ± 10.93	511.62± 22.31*	0.0252
LVEDD, mm	3.56±0.06	3.60±0.10	0.7560
LVESD, mm	2.02±0.04	2.12±0.08	0.3131
LVPWd, mm	0.77±0.01	0.76±0.01	0.7207
LVPWs, mm	1.28±0.01	1.26±0.01	0.1750
FS, %	43.16±0.83	41.01 ± 1.52	0.2367
r/h	2.32±0.05	2.36±0.05	0.6864

The HR of both groups remained in the normal HR range for healthy adult mice (n=8 per group, unpaired t-test, *p<0.05 in comparison to control). Data are presented as mean ± SEM. FS, fractional shortening; HR, heart rate; L VEDD, left ventricular end-diastole diameter; L VESD, left ventricular end-systole diameter; LVPWd, left ventricular posterior wall thickness at diastole; L VPW s, left ventricular posterior wall thickness at systole; r/h, left ventricular radius to left ventricular posterior wall thickness ratio.

TABLE 3.

Echocardiographic assessment of cardiac function in the empagliflozin group at baseline and after 6 weeks 0f treatment with vehicle demonstrated a marginal reduction in left ventricular posterior wall thickness at diastole between the two measurements

EMPA	***Baseline, n= 8***	***6 Weeks, n=8***	***p***
HR, beats/min	538.41 ± 10.63	511.62±22.31	0.3566
LVEDD, mm	3.70±0.06	3.60±0.10	0.4155
LVESD, mm	2.19±0.05	2.12±0.08	0.5104
LVPWd, mm	0.78±0.01	0.76±0.01*	0.0306
LVPWs, mm	1.28±0.01	1.26±0.01	0.2753
FS, %	40.56±0.64	41.01 ±1.52	0.8255
r/h	2.35±0.06	2.36±0.05	0.9163

Data are presented as mean ± SEM. n = 8, paired t-Test, *p < 0.05 in comparison to baseline.

FIG. 1.

Acute administration of EMPA does not reduce infarct size in nondiabetic animals.

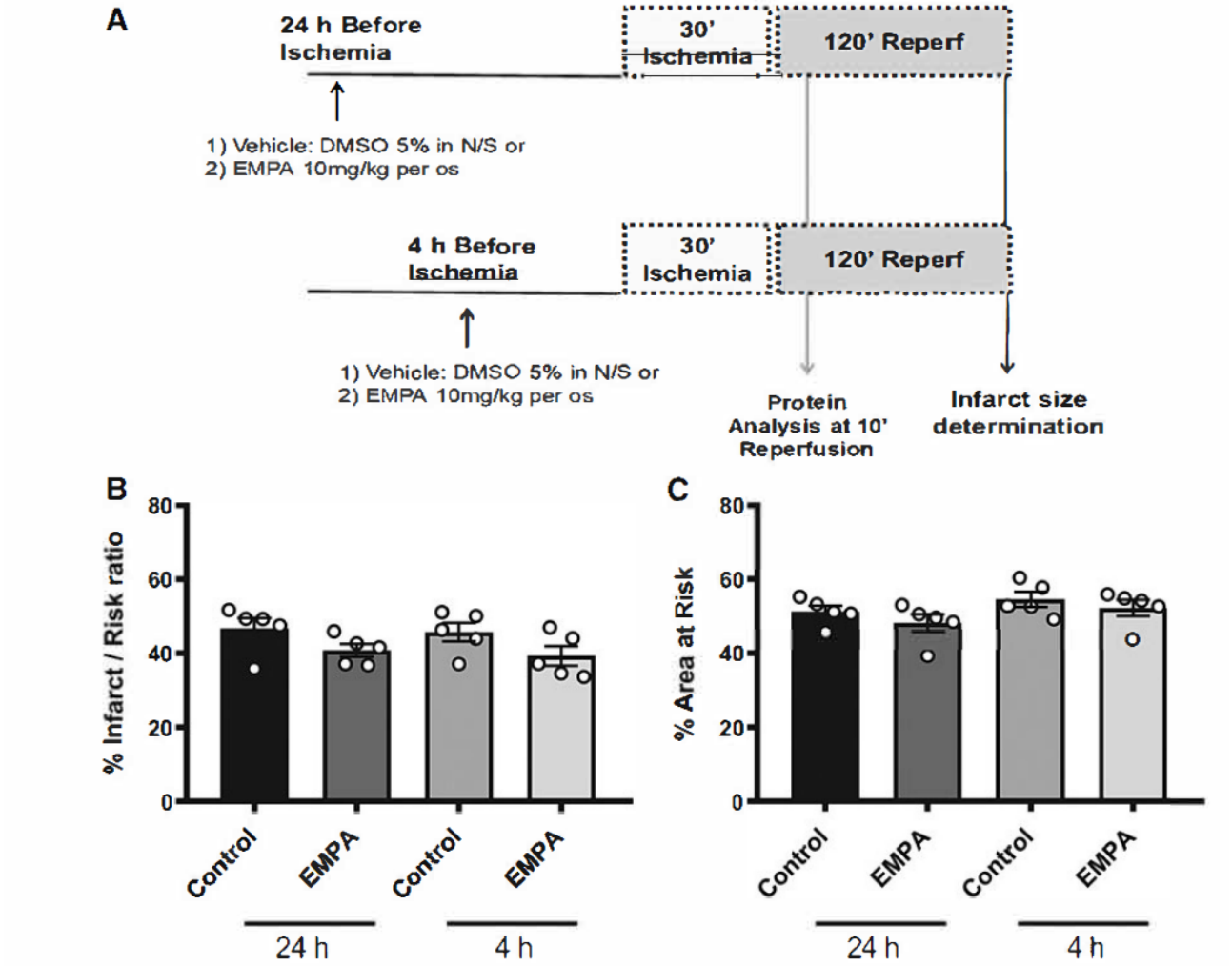

(A) Schematic representation of protocols with acute EMPA treatment. (B) Representative graphs of Infarct/Risk ratio%. The values for each animal are presented as a scatter plot (means ± SEM). (C) Bar graph of the % area at risk (p=NS, n=5 per group). Unpaired t-test between the EMPA-treated groups and their respective controls was performed. EMPA, empagliflozin; SEM, standard error of the mean.

Fig. 2

Chronic administration of EMPA reduces myocardial infarct size in nondiabetic mice without affecting body weight, circulating glucose levels, and blood pressure.

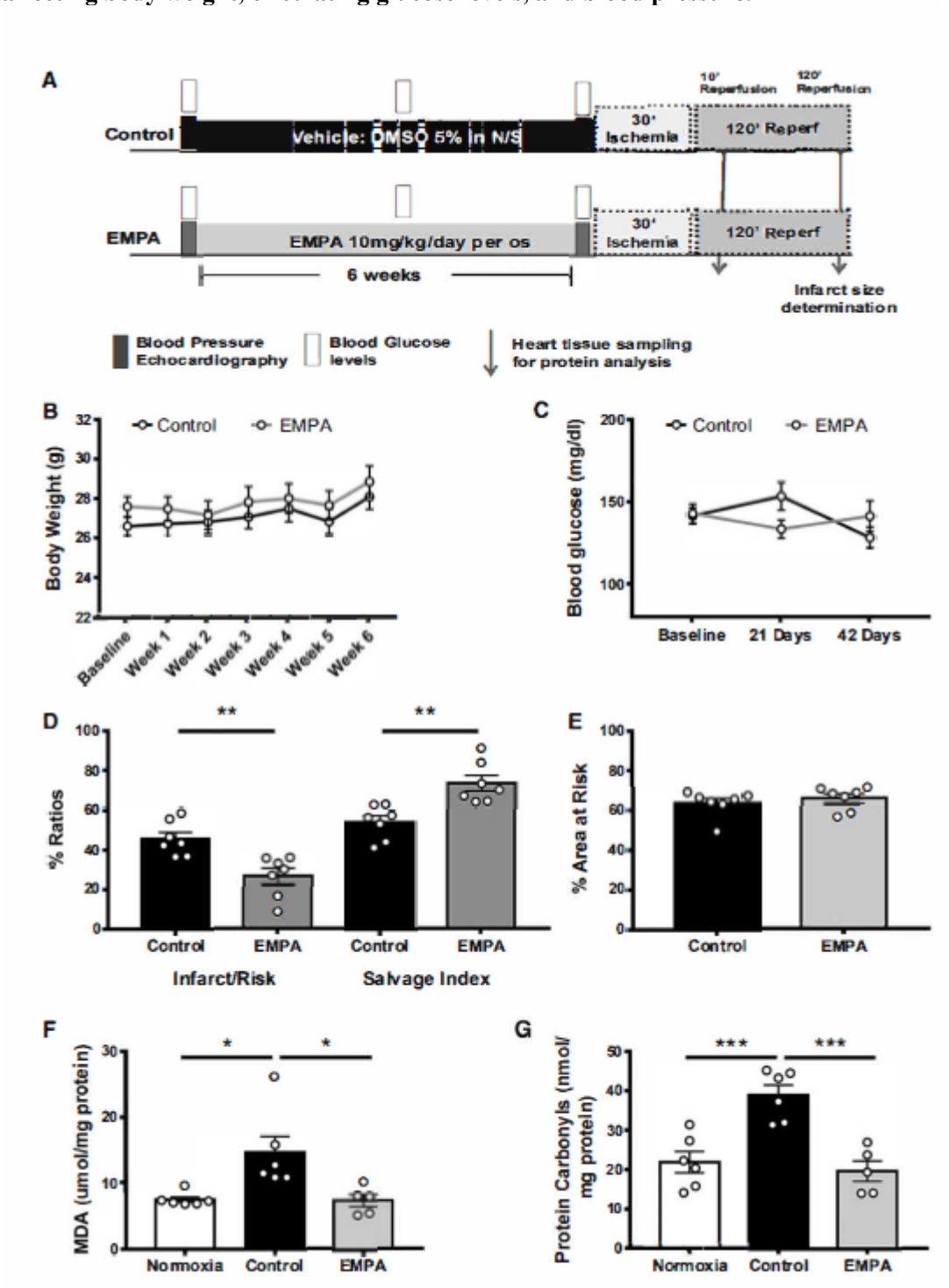

(A) Illustration of the experimental protocol of chronic administration of EMPA. The interventions that were performed are depicted with different symbols or patterns, as explained in the figure. (B) Time course graph of mean mice weight per week enrolled in the EMPA group depicted in gray versus the vehicle- treated group depicted in black (p=NS). Dots represent means ± SEM for each time-point. (C) Time course graph of the fasting glucose levels (mM) of the animals enrolled in the EMPA group depicted in gray in comparison to the control group illustrated with the black line (p=NS) (n=8 per group, two-way ANOVA was employed). Dots represent means ± SEM for each time-point. (D) Representative graphs of Infarct/Risk ratio% (**p <

0.01 vs. control) and Salvage Index% (**p < 0.01 vs. control). The values for each animal are presented as a scatter plot (means ± SEM). (E) Bar graph of the % area at risk (p=NS) (n=7 per group). Unpaired t-test between the two groups was performed. (F) Myocardial MDA levels (μmol/mg protein). *p < 0.05. (G) Myocardial PCs levels (nmol/mg protein). ***p < 0.001. The values for each animal are presented as a scatter plot (means ± SEM). ANOVA, analysis of variance; MDA, malondialdehyde; PCs, protein carbonyls.

FIG. 3.

Chronic administration of EMPA is cardioprotective through an increase in p(Y705)STAT-3 at the 10th minute of reperfusion.

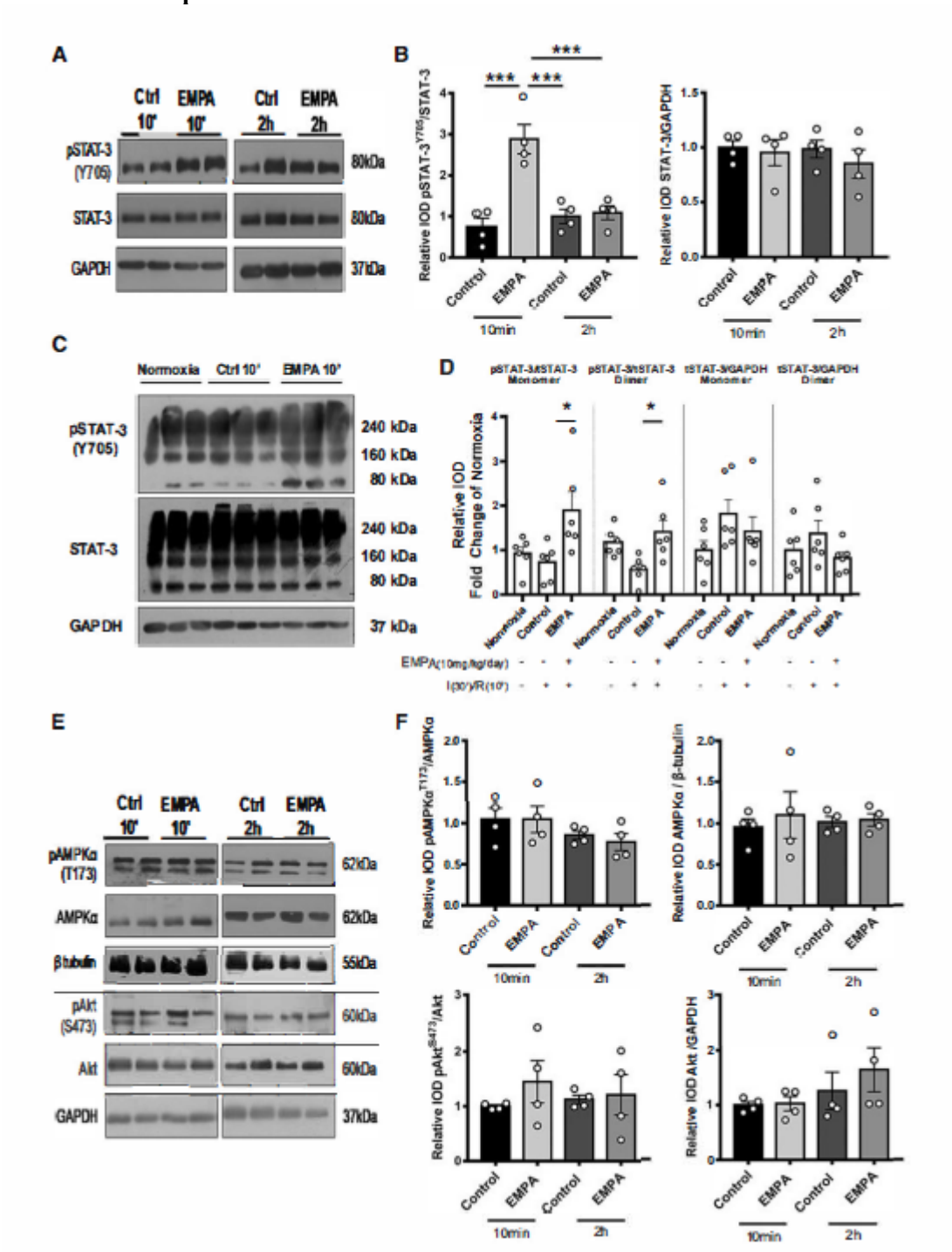

(A) Representative Western blots of p(Y705)STAT-3/STAT-3 and STAT-3/GAPDH (***p < 0.001) and (B)

relative densitometric graphs at the 10th minute and 2 h of reperfusion after normalization to total protein are presented. Dots represent biological replicates (n = 4 per group, unpaired t-test was performed for each time point). (C) Representative Western blots of p(Y705)STAT-3/STAT-3 and STAT-3/GAPDH under nonreducing conditions. (D) Relative densitometric graphs at the 10th minute of reperfusion after normalization to total protein are presented. Dots represent biological replicates (n = 6 per group, one-way ANOV A with Tukey as post hoc test among the three groups was performed for each band). *p<0.05. (E) Representative Western blots of p(Tl73)AMPKα/AMPKα, p(S473)Akt/Akt, AMPKα/β-tubulin, and Akt/GAPDH. (F) Relative densitometric graphs of p(Tl73)AMPKα/AMPKα, p(S473)Akt/Akt, AMPKα/β-tubulin, and Akt/GAPDH at the 10th and 2 h of reperfusion after normalization to total protein (n=4 per group, p=NS, unpaired t-test was performed for each time point). Akt, protein kinase B; AMPKα, adenosine monophosphate-activated protein kinase α; GAPDH, glyceraldehyde-3-phosphate dehydrogenase; STAT-3, signal transducer and activator of transcription 3.

FIG. 4.

Acute administration of EMPA at 4 or 24 h before the ischemic insult does not alter STAT-3 hosphorylation.

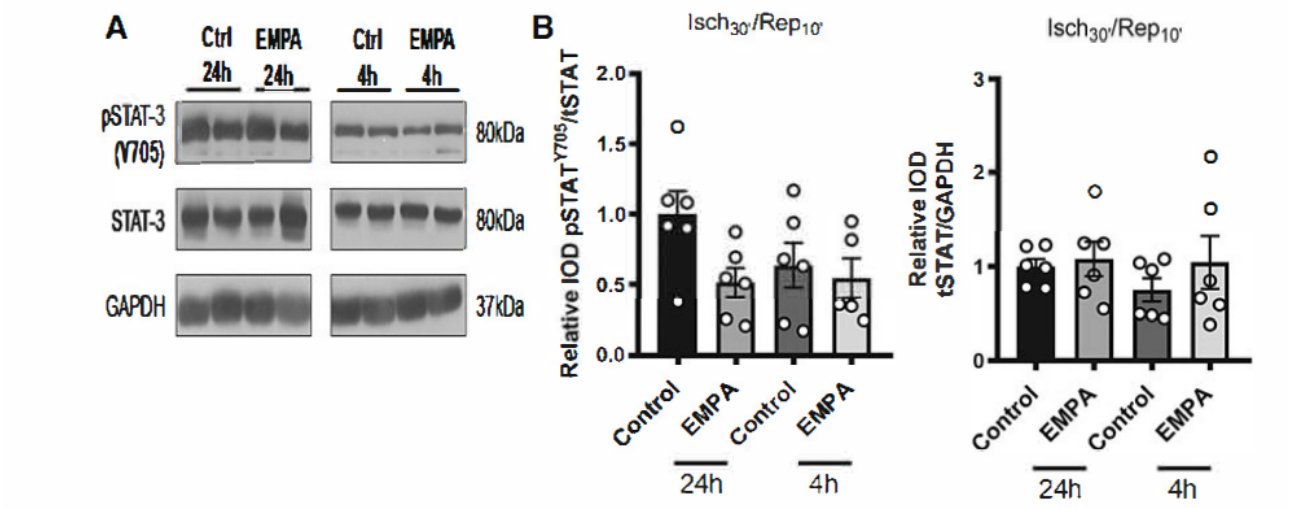

(A) Representative Western blots of p(Y705)STAT-3/STAT-3 and STAT-3/GAPDH for the acute administration protocols. (B) Relative densitometric graphs at the 10th minute of reperfusion after normalization to total protein of p(Y705) STAT-3/STAT-3 and STAT-3/GAPDH (p = NS) are presented. Dots represent biological replicates (n = 5 per group. Unpaired t-test was performed between the EMPA groups and their respective controls).

FIG. 5.

Proteomic analysis after 6-week EMPA treatment at the 10th minute of reperfusion.

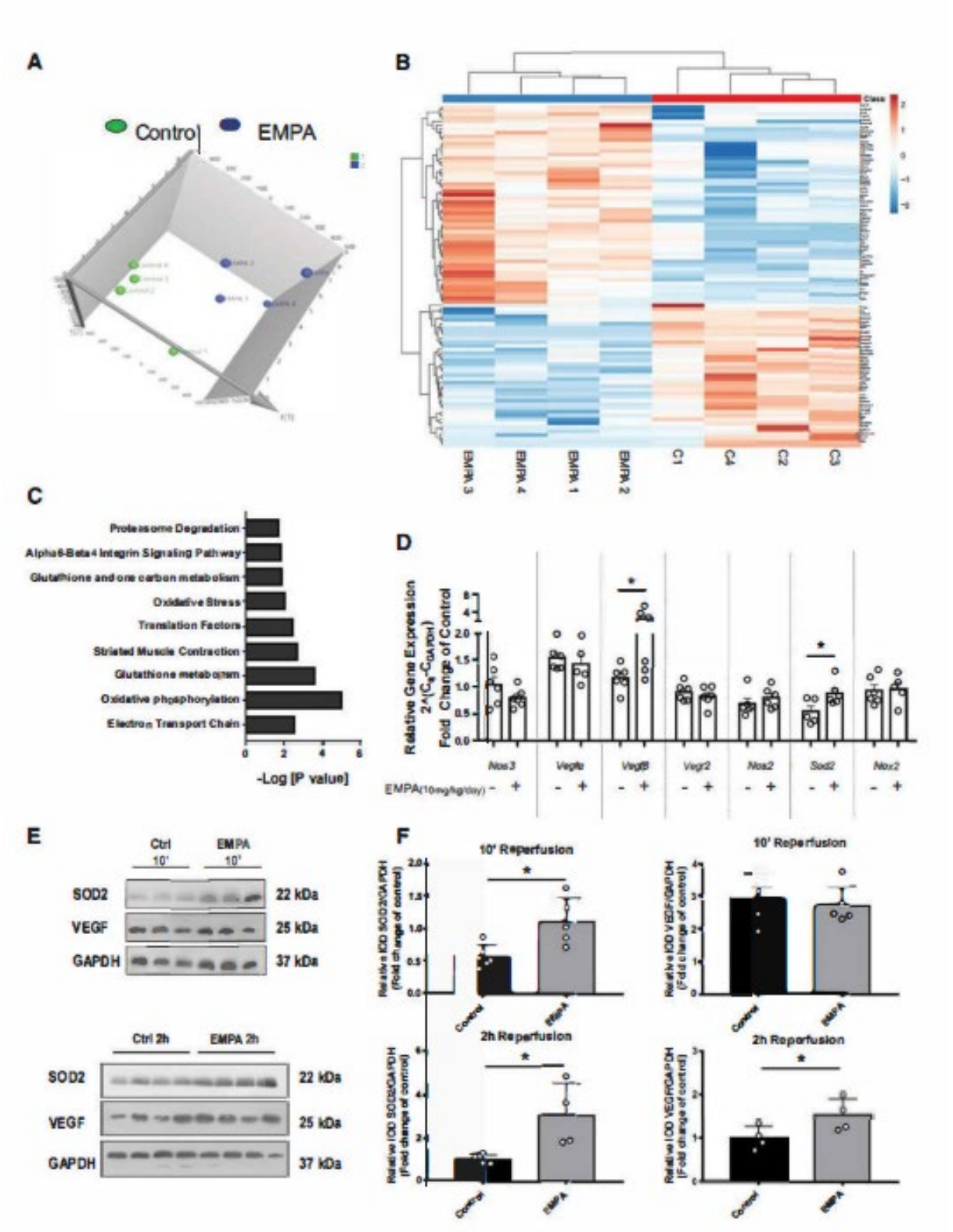

(A) Principal component analysis of the reperfused heart proteome was performed in an unsupervised fashion. The normalized area of the total protein identifications for each anima! was used in this analysis. The scatter plot illustrates the first three principal component scores in a three-dimensional space. Two clusters are inferred, indicating the absence of outlying samples estimated by SIMCA P + 11.5. (B) Tue heatmap illustrates the expression level changes of the 93 statistically significant proteins between the control and EMPA groups. (C) WEB-based GEne SeT AnaLysis was employed to translating gene lists into

biological insights. Tue dataset of 373 differentially expressed and statistically significant proteins is mapped to representative molecular pathways. (D) Real-time PCR data of mRNA expression of Nos3, Vegfα, Vegfβ, Vegfr2, Nos2, and Nox2 genes in I/R-operated animals (at the 10th minute of reperfusion) treated with vehicle or EMPA. Relative gene expression is calculated by the standard formula $2^{\wedge(Cq - CTGAPDH)}$; fold change of control and data are presented as mean±SEM (n=5-6 per group; *p<0.05, unpaired, two-tailed, Student's t-test). (E) Representative Western blots of SOD2/GAPDH and VEGF/GAPDH at the 10th minute and 2 h of reperfusion. (F) Relative densitometric graphs at the 10^{th} minute and 2 h reperfusion after normalization to total protein are presented. Dots represent biological replicates (n = 6 per group and n=4 per group respectively; *p<0.05, unpaired, two-tailed, Student's t-test). I/R, ischemia-reperfusion; Nos2, inducible nitric oxide synthase; Nos3, endothelial nitric oxide synthase; Nox2, NAPDH oxidase 2; SOD2, superoxide dismutase 2; VEGF, vascular endothelial growth factor.

FIG. 6.

Vessel formation detected on murine hearts on chronic administration of EMPA and increased HMEC viability dependent on STAT-3 activation.

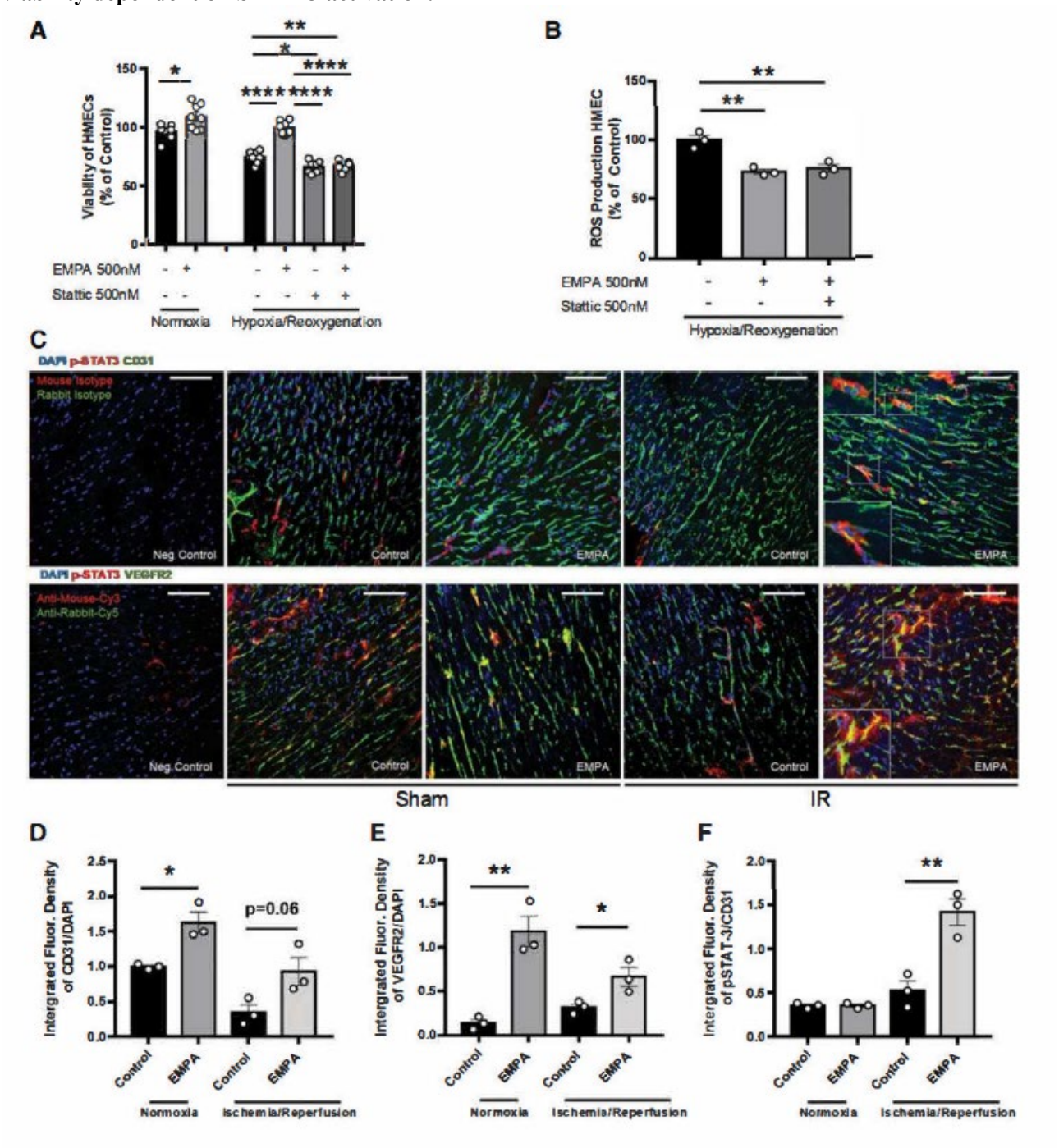

(A) Cell viability % using the MTT assay of HMEC cells on 24 h of treatment with EMP A. Two experimental settings, namely normoxia and 3 h hypoxia and 1 h reoxygenation, are depicted. The panel below the graph depicts the cell treatments per group. Dots represent different experiments. Unpaired, two-tailed Student's t-test and one-way ANOVA were performed with Tukey as post hoc test (*p<0.05, **p<0.0l,****p<0.0001 in comparison to control group or as depicted). (B) % ROS production of HMEC cells after 3 h of hypoxia and 1 h of reoxygenation on the illustrated treatments. One-way ANOV A was performed with Tukey as post hoc test (n = 3 independent experiments, **p<0.01 in comparison to control group or as depicted). (C) Upper panel: Representative images of CD31, pSTAT-3(Y705), and DAPI staining after 6 weeks of EMPA treatment (sham-operated groups) and in the infarcted hearts of the vehicle- and EMPA-treated mice at the 10th minute of reperfusion. Lower panel: Representative images of VEGFR2,

pSTAT-3(Y705), and DAPI staining after 6 weeks of EMPA treatment (sham-operated groups) and in the infarcted hearts of the vehicle- and EMPA-treated mice at the 10th minute of reperfusion. Scale bar= 100 µm. (D) Integrated fluorescent density of CD31/DAPI. Unpaired, two-tailed Student's t-test between control and EMPA group in two different experimental settings (n = 3, *p < 0.05). (E) Integrated fluorescent density of VEGFR2/DAPI. Unpaired, two-tailed Student's t-test between control and EMPA group in two different experimental settings (n=3, *p<0.05, **p<0.01). (F) Integrated fluorescent density of p(Y705) STAT-3/CD31. Unpaired, two-tailed Student's t-test between control and EMPA group in two different experimental settings (n = 3, **p < 0.01). DAPI, 4',6-diamidino-2-phenylindole; HMEC, human microvascular endothelial cell; MTT, 3-(4,5-dimethylthiazol-2-yl)-2,5-diphenyltetrazolium bromide.

FIG. 7.

Schematic illustration of the cardioprotective mechanism of chronic EMPA treatment on nondiabetic mice.

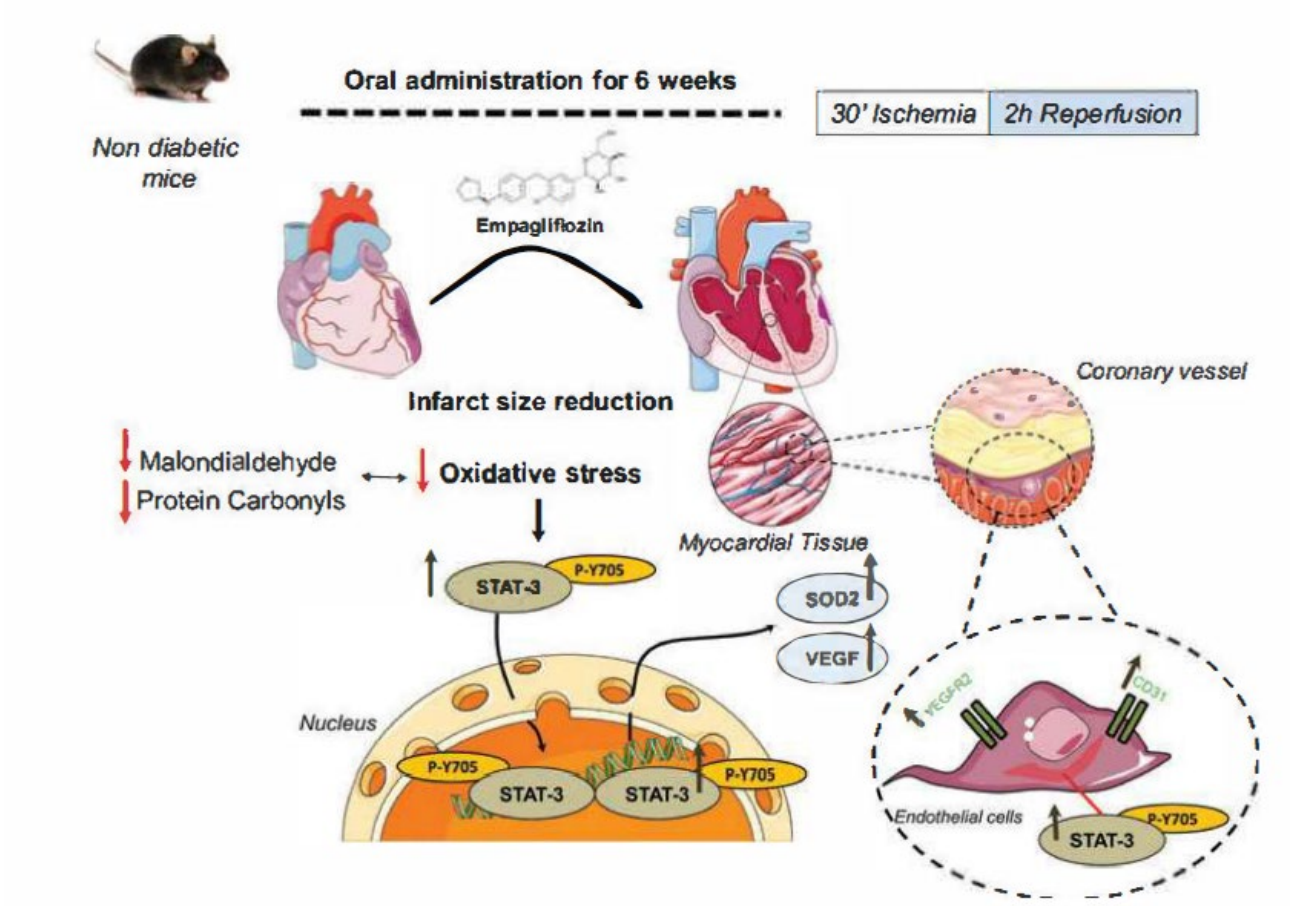

EMPA reduces infarct size after 6 weeks of oral administration in nondiabetic mice. Chronic EMPA administration reduces cardiac oxidative stress as is evident by the markers of lipid and protein oxidation of MDA and PCs and it activates STAT-3 through Y(705) phosphorylation. The EMPA treatment induces p(Y705)STAT-3 dimerization at early reperfusion, and, therefore, the downstream proteins SOD2 and VEGF are upregulated. In parallel, EMPA increases survival of endothelial cells in a STAT-3 dependent manner. The endothelial cell markers CD31 and VEGFR2 and the pSTAT-3(Y705) signal derived from endothelial cells are boosted at early reperfusion.